



CERN-EP-2023-264
17 November 2023

Multiplicity dependence of charged-particle intra-jet properties in pp collisions at $\sqrt{s} = 13$ TeV

ALICE Collaboration*

Abstract

The first measurement of the multiplicity dependence of intra-jet properties of leading charged-particle jets in proton–proton (pp) collisions is reported. The mean charged-particle multiplicity and jet fragmentation distributions are measured in minimum-bias and high-multiplicity pp collisions at center-of-mass energy $\sqrt{s} = 13$ TeV using the ALICE detector. Jets are reconstructed from charged particles produced in the midrapidity region ($|\eta| < 0.9$) using the sequential recombination anti- k_T algorithm with jet resolution parameters $R = 0.2, 0.3,$ and 0.4 for the transverse momentum (p_T) interval 5–110 GeV/ c . The high-multiplicity events are selected by the forward V0 scintillator detectors. The mean charged-particle multiplicity inside the leading jet cone rises monotonically with increasing jet p_T in qualitative agreement with previous measurements at lower energies. The distributions of jet fragmentation functions z^{ch} and ξ^{ch} are measured for different jet- p_T intervals. Jet- p_T independent fragmentation of leading jets is observed for wider jets except at high- and low- z^{ch} values. The observed “hump-backed plateau” structure in the ξ^{ch} distribution indicates suppression of low- p_T particles. In high-multiplicity events, an enhancement of the fragmentation probability of low- z^{ch} particles accompanied by a suppression of high- z^{ch} particles is observed compared to minimum-bias events. This behavior becomes more prominent for low- p_T jets with larger jet radius. The results are compared with predictions of QCD-inspired event generators, PYTHIA 8 with Monash 2013 tune and EPOS LHC. It is found that PYTHIA 8 qualitatively reproduces the jet modification in high-multiplicity events except at high jet p_T . These measurements provide important constraints to models of jet fragmentation.

arXiv:2311.13322v1 [hep-ex] 22 Nov 2023

© 2023 CERN for the benefit of the ALICE Collaboration.

Reproduction of this article or parts of it is allowed as specified in the CC-BY-4.0 license.

*See Appendix A for the list of collaboration members

1 Introduction

Hadronic and nuclear collisions at ultra-relativistic energies are the subject of intense research in the field of high-energy physics, as they enable the study of the fundamental constituents of matter and the forces that govern their interactions. The energy density achieved in the laboratory by colliding high-energy nucleus beams is sufficient to allow the confined hadronic matter to get transformed into a hot and dense state of quantum chromodynamics (QCD) [1] matter where partons are no longer confined into hadrons, known as quark–gluon plasma (QGP) [2–5]. Several experiments at RHIC and the LHC are being performed to study the physics of this strongly-interacting QCD matter. Various experimental signatures have been observed in heavy-ion (A–A) collisions in favor of the formation of the QGP medium. Jet quenching [6–8], which is particularly manifest as in-medium energy loss of energetic partons [9–12], is one of the most important signatures among them.

Jets are cascades of energetic hadrons that result from the fragmentation of hard-scattered (i.e. produced in processes with large squared momentum transfer Q^2) quarks and gluons in high-energy collisions. In proton–proton (pp) collisions, measurements of jet production provide a testbench of perturbative calculations and help to study non-perturbative effects in QCD [13–17]. In addition, measurements in pp collisions also provide the baseline for similar measurements in A–A collisions. Jet production is found to be suppressed, and jet properties are also modified with respect to those in pp collisions due to the presence of hot and dense QCD matter in A–A collisions. The phenomenon is known as jet quenching in heavy-ion collisions. In particular, highly energetic jets, while passing through the QGP medium, lose energy via elastic scatterings and medium-induced gluon radiations.

Interestingly, recent measurements of high-multiplicity pp and p–Pb (proton-lead) collisions show ample signatures conventionally associated with the QGP formation in heavy-ion collisions. These observations triggered an immense research interest to look for the onset of QGP-like effects in high-energy small collision systems, particularly at high multiplicity, through a plethora of new and precise measurements of different potential observables [18–25]. Measurements primarily related to the soft QCD sector of particle production mechanisms have brought to the forefront various observations commonly understood as due to medium formation such as the long-range ridge-like structure at the near side in two-particle angular correlations [26–30], strangeness enhancement [31–33], and elliptic flow (v_2) [34, 35]. However, in terms of the hard probes, no conclusive evidence of jet quenching has been found yet within the current precision achieved in experiments [36, 37]. This brings to the table the possibility of QGP formation in small collision systems as an open question that requires to be addressed and investigated further. In view of this, intra-jet properties such as jet shape and fragmentation functions are promising observables since they are more sensitive to the details of the parton shower and hadronization processes in QCD [38–41].

Numerous measurements of intra-jet properties have been performed in hadronic collisions. Jet shape observables were previously measured by the CDF [42, 43] and D0 [44] Collaborations in $p\bar{p}$ collisions at the Tevatron and by the ALICE [13], ATLAS [45, 46], and CMS [47, 48] Collaborations in pp collisions at the LHC. Measurements of jet fragmentation functions have also been reported by the CDF Collaboration [49] in $p\bar{p}$ collisions, whereas ALICE [13, 14], ATLAS [46, 50, 51], and CMS [52] Collaborations have also studied jet fragmentation functions in pp and Pb–Pb (lead-lead) collisions at LHC energies.

This article presents the first measurement of the multiplicity dependence of charged-particle intra-jet properties in pp collisions at $\sqrt{s} = 13$ TeV. In this study, the average jet constituent multiplicity $\langle N_{\text{ch}} \rangle$ and the two variables commonly used to describe the jet fragmentation functions (z^{ch} and ξ^{ch}) are measured for leading charged-particle jets (jet with the highest p_{T} in an event) with jet resolution parameters $R = 0.2, 0.3,$ and 0.4 as a function of jet p_{T} in minimum-bias (MB) and high-multiplicity (HM) pp collisions using the ALICE detector at the LHC. Leading charged-particle jets are considered since they are theoretically well-defined objects and less prone to experimental effects compared to inclusive jets [53]. Moreover, the formation and evolution of leading jets can be described by jet functions which satisfy

non-linear DGLAP-type evolution equations and therefore they are comparable with the QCD hard scattering models [42].

This paper is organized as follows: Section 2 describes the experimental setup of the ALICE detector and the data samples used in this study. Details of jet reconstruction and jet observables are discussed in Sec. 3. The procedures applied to correct the measured distributions for instrumental effects and underlying event contaminations are presented in Sec. 4. Section 5 outlines the estimation of systematic uncertainties from various sources. Results are presented and discussed in detail in comparison with predictions from QCD-inspired event generators in Sec. 6 and the conclusions are summarized in Sec. 7.

2 Experimental setup, data sets, and event selection

This analysis uses the data from pp collisions at $\sqrt{s} = 13$ TeV collected in 2016, 2017, and 2018 with the ALICE detector at the LHC. The ALICE detector and its performance are described in detail in Refs. [54, 55]. Events are selected using the information from two V0 scintillator detectors [56], which cover an azimuthal acceptance of $0 < \phi < 2\pi$ and pseudorapidity $2.8 < \eta < 5.1$ (V0A) and $-3.7 < \eta < -1.7$ (V0C), respectively. The online trigger for MB events requires the coincidence of signals both in the V0A and V0C detectors, while the high-multiplicity sample is collected using a HM trigger condition [57] that requires the V0M signal amplitude (sum of V0A and V0C signal amplitudes) to be greater than 5 times of its mean signal amplitude $\langle \text{V0M} \rangle$ in MB events [58]. Charged-particle tracks are reconstructed in the midrapidity region ($|\eta| < 0.9$) utilizing the information from two central barrel detectors, the Inner Tracking System (ITS) and the Time Projection Chamber (TPC) placed inside a large solenoidal magnet with a uniform magnetic field of $B = 0.5$ T [55] and field lines along the beam direction. The primary vertex of the collision is reconstructed from tracks. Events with a primary vertex outside ± 10 cm along the beam direction from the nominal interaction point are rejected to guarantee a uniform acceptance of the central barrel detectors. Events with collision pileup are removed by rejecting events with multiple reconstructed vertices [55, 59]. The results presented in this paper are based on 1832 million MB and 870 million HM events corresponding to integrated luminosities of 32 nb^{-1} and 10 pb^{-1} respectively.

The analysis is carried out using the primary charged particles, defined as all particles with a mean proper lifetime $\tau > 1 \text{ cm}/c$, which are either produced directly in the interaction or from decays of particles with mean proper lifetime $\tau < 1 \text{ cm}/c$ [60]. Jets are reconstructed from charged-particle tracks measured with the ITS and TPC detectors. To ensure an approximately uniform azimuthal acceptance and good momentum resolution, charged tracks are reconstructed using a hybrid selection technique [59, 61], where two different classes of tracks are combined. In the first class, tracks are required to include at least one hit in the silicon pixel detector (SPD), which equips the two innermost layers of the ITS. The second class contains tracks without hits in the SPD, where the primary vertex is used as an initial point of the trajectory to improve the estimation of the particle momentum. Tracks with transverse momentum $p_T > 0.15 \text{ GeV}/c$ in the pseudorapidity range $|\eta| < 0.9$ over the full azimuth ($0 < \phi < 2\pi$) are considered in this analysis. The hybrid track reconstruction efficiency in both MB and HM events is found to be about 85% at $p_T = 1 \text{ GeV}/c$, decreasing to 74% at $p_T = 50 \text{ GeV}/c$. Primary-track momentum resolution is 0.7% at $p_T = 1 \text{ GeV}/c$, increasing to 3.7% at $p_T = 50 \text{ GeV}/c$.

The corrections for instrumental effects and the evaluation of systematic uncertainties are performed with the help of simulations based on Monte Carlo (MC) event generators PYTHIA 8 [62] with Monash 2013 tune [63] (hereafter referred to as PYTHIA 8) and EPOS LHC [64]. The selections of MB and HM events in the simulated data are the same as in experimental data.

3 Jet reconstruction and jet observables

Charged-particle jets are reconstructed from charged-particle tracks with $p_T > 0.15$ GeV/ c and $|\eta| < 0.9$ using the anti- k_T algorithm [65] with resolution parameters $R = 0.2, 0.3,$ and 0.4 using FastJet 3.2.1 [66]. The pseudorapidity coverage of the reconstructed jets is limited within the fiducial acceptance of the TPC, $|\eta_{\text{jet}}| < (0.9 - R)$, to minimize the TPC edge effects in jet reconstruction. Leading jets within the p_T interval 5–110 GeV/ c are considered for this analysis.

The performance of jet reconstruction is studied using PYTHIA 8. Particles produced directly from the MC event generator (truth-level) are transported through a GEANT 3 [67] simulation of the ALICE detector system to obtain the reconstructed tracks (detector-level). Truth-level particles (detector-level tracks) are used to reconstruct the truth-level (detector-level) jets by applying the same algorithms and kinematic selections as in data. Detector-level leading jets are matched to the geometrically closest truth-level jets and a one-to-one matching is ensured between them. The axes of the matched jets are required to be within $\Delta R < 0.6R$ to minimize unrealistic matching. The matched jets are used to calculate the jet energy scale $\text{JES} = (p_{T,\text{det}}^{\text{jet, ch}} - p_{T,\text{truth}}^{\text{jet, ch}})/p_{T,\text{truth}}^{\text{jet, ch}}$, jet energy resolution $\text{JER} = \sigma(p_{T,\text{det}}^{\text{jet, ch}})/p_{T,\text{truth}}^{\text{jet, ch}}$ (where σ is the width of the $p_{T,\text{det}}^{\text{jet, ch}}$ distribution for a given value of $p_{T,\text{truth}}^{\text{jet, ch}}$), and jet reconstruction efficiency ϵ_{reco} for $R = 0.2, 0.3,$ and 0.4 , where $p_{T,\text{truth}}^{\text{jet, ch}}$ and $p_{T,\text{det}}^{\text{jet, ch}}$ denote the transverse momentum of truth- and detector-level jets, respectively. The JES distribution shows a peak at zero with an asymmetric tail towards negative values due to tracking inefficiencies, which is characterized by the mean value of JES denoted as Δ_{JES} . Table [1] summarizes the values of Δ_{JES} , JER, and ϵ_{reco} for different jet- p_T ranges.

Table 1: Approximate values of Δ_{JES} , JER, and ϵ_{reco} to characterize the jet reconstruction performance for jet $R = 0.2, 0.3,$ and 0.4 .

$p_{T,\text{truth}}^{\text{jet, ch}}$ (GeV/ c)	$R = 0.2$			$R = 0.3$			$R = 0.4$		
	Δ_{JES} (%)	JER (%)	ϵ_{reco} (%)	Δ_{JES} (%)	JER (%)	ϵ_{reco} (%)	Δ_{JES} (%)	JER (%)	ϵ_{reco} (%)
10–20	-9	20	89	-10	20	90	-12	20	91
20–30	-11	21	94	-12	20	95	-13	20	95
30–40	-13	21	95	-14	20	96	-14	20	96
40–50	-14	21	96	-15	20	97	-15	20	97
80–90	-18	23	97	-19	22	97	-18	22	97

The intra-jet properties such as mean charged-particle multiplicity within a jet cone and the jet fragmentation functions, z^{ch} and ξ^{ch} are measured for leading jets in both minimum-bias and high-multiplicity pp collisions. The number of charged particles found within the jet cone is termed charged-particle multiplicity N_{ch} . The mean charged-particle multiplicity $\langle N_{\text{ch}} \rangle$ is calculated and presented as a function of the leading jet p_T . The jet fragmentation functions, z^{ch} and ξ^{ch} are defined as:

$$z^{\text{ch}} = \frac{p_T^{\text{particle}}}{p_T^{\text{jet, ch}}}, \quad (1)$$

$$\xi^{\text{ch}} = \ln \left(\frac{1}{z^{\text{ch}}} \right), \quad (2)$$

where p_T^{particle} is the transverse momentum of the jet constituent. The distributions are normalized by the total number of leading jets and explicitly describe the energy sharing between constituents within a jet. The ξ^{ch} distribution is complementary to z^{ch} , which emphasizes fragmentation into low momentum constituents and is particularly suited to illustrate the QCD coherence effects [40, 68].

4 Corrections

4.1 Unfolding

The measured distributions are corrected for instrumental effects such as limited track reconstruction efficiency, finite track- p_T resolution, and particle–material interactions using an iterative method based on Bayes’ theorem [69] implemented in the RooUnfold package [70]. To account for these effects, a 4D response matrix (RM) is constructed from simulated data and considered as an input to the unfolding procedure, which maps between the truth- and detector-level jet observables. Before the construction of the response matrix, the jets at the truth- and detector-level are matched as described in Sec. 3. The elements of the 4D response matrix are $p_{T,\text{det}}^{\text{jet, ch}}$, Obs_{det} , $p_{T,\text{truth}}^{\text{jet, ch}}$ and Obs_{truth} , where $p_{T,\text{det}}^{\text{jet, ch}}$ and $p_{T,\text{truth}}^{\text{jet, ch}}$ are detector- and truth-level jet p_T and Obs_{det} and Obs_{truth} stand for the observables, $Obs \in \{N_{\text{ch}}, z^{\text{ch}}, \xi^{\text{ch}}\}$. For z^{ch} and ξ^{ch} , the truth- and detector-level jet constituents are also matched before constructing the response matrices. Any detector-level (truth-level) jet constituent without an associated matched truth-level (detector-level) jet constituent is termed fake (miss) and is fed to the response matrix in addition to the matched jet constituents to account for the efficiency and purity of the constituent matching procedure. The unfolded distributions obtained using the Bayesian unfolding technique primarily depend on two important factors, the regularization parameter and the prior distribution. In the case of Bayesian unfolding, the regularization parameter is the number of iterations. The regularization parameter is tuned to reduce the variance of the unfolded distribution. The truth-level distributions are provided as the prior in the unfolding process that gets updated in subsequent iterations.

Two types of closure tests are performed to validate the unfolding procedure, known as statistical and shape closure tests. In the statistical closure test, two statistically independent simulated datasets are considered, where the response matrix is built from one sample, and the truth- and detector-level distributions of N_{ch} , z^{ch} , and ξ^{ch} are obtained from the other sample. The detector-level distributions are then unfolded and compared with the truth-level distribution to check the robustness of the unfolding procedure against the statistical fluctuations in the data. In the shape closure test, a similar approach as the statistical closure is applied, however, the response matrix is reweighted with the ratio between the measured distribution and the one from detector-level MC. Then, the unfolded distribution is compared with truth-level distributions to check the robustness of the unfolding against the change in the shape of distributions. Proper closure is found in both tests within the statistical uncertainties.

4.2 Underlying event subtraction

The underlying event (UE) consists of all particles produced in the collision that are not an integral part of the jet or produced directly from the hard scattering. In pp collisions, some of the important sources of UE are beam remnants, multiparton interactions, initial- and final-state radiations. The perpendicular cone method used in Refs. [13, 14] is adopted to estimate UE and correct the corresponding distributions of jet observables in both MB and HM events.

In this approach, the UE particle yield is measured event-by-event within a cone of the same radius as the jet resolution parameter located at the same pseudorapidity as the leading jet, but in the direction perpendicular to the leading jet axis. The information of particles within the perpendicular cone is used to estimate the UE contributions to the jet observables.

The UE distributions of N_{ch} , z^{ch} , and ξ^{ch} are corrected for the instrumental effects using the unfolding procedure discussed in Sec. 4.1. After unfolding, the unfolded UE distributions are subtracted from the unfolded signal distributions on a statistical basis, however, a simultaneous correction for the UE contribution to the jet transverse momentum is not applied here [13, 14]. The estimated UE contribution for $\langle N_{\text{ch}} \rangle$ in MB events is comparable with the values reported in Ref. [71].

5 Systematic uncertainties

The systematic uncertainties associated with the unfolded distributions are mainly arising from the uncertainties in track reconstruction efficiency, the unfolding procedure (variation in the regularization parameter of unfolding, change of prior distribution, and bin truncation), the choice of MC model in the correction procedure, and the uncertainty in the estimation of the UE. For each of these sources, a modified response matrix that incorporates the variation due to the respective uncertainties is built (as described below) and used to unfold the measured distribution. The difference between the corrected distributions unfolded with the default and modified response matrices is quoted as the corresponding systematic uncertainty. The total systematic uncertainty is calculated by taking the quadrature sum of all the individual sources, assuming that all the sources are uncorrelated.

Table 2: Summary of systematic uncertainties (in %) on $\langle N_{\text{ch}} \rangle$ for selected intervals of jet p_{T} for jet $R = 0.2, 0.3,$ and 0.4 in MB and HM events.

Sources	Systematic uncertainties on $\langle N_{\text{ch}} \rangle$ for MB (%)								
	$R = 0.2$			$R = 0.3$			$R = 0.4$		
	Jet p_{T} in GeV/c			Jet p_{T} in GeV/c			Jet p_{T} in GeV/c		
	5–10	45–50	90–110	5–10	45–50	90–110	5–10	45–50	90–110
Track reconst. efficiency	0.9	2.0	2.5	1.3	2.1	2.2	1.8	2.5	2.4
Unfolding parameter	negl.	0.1	negl.	0.1	0.1	0.2	0.1	negl.	0.1
Prior change	negl.	0.5	negl.	0.1	0.2	0.3	0.1	0.2	0.2
Bin truncation	10.4	0.3	2.2	11.3	0.3	1.2	11.1	0.3	1.1
MC generator	1.0	1.4	10.2	1.0	1.9	3.2	0.8	2.2	4.0
UE	0.1	0.1	negl.	0.3	0.2	0.7	0.7	0.4	0.8
Total	10.5	2.5	10.7	11.4	2.9	4.2	11.3	3.4	4.9

Sources	Systematic uncertainties on $\langle N_{\text{ch}} \rangle$ for HM (%)								
	$R = 0.2$			$R = 0.3$			$R = 0.4$		
	Jet p_{T} in GeV/c			Jet p_{T} in GeV/c			Jet p_{T} in GeV/c		
	5–10	45–50	90–110	5–10	45–50	90–110	5–10	45–50	90–110
Track reconst. efficiency	1.1	1.5	2.4	2	2.3	2.6	2.5	2.4	3.4
Unfolding parameter	negl.	0.1	0.1	negl.	0.1	0.1	0.1	0.1	0.1
Prior change	negl.	0.1	0.3	negl.	0.1	1.4	0.2	0.1	0.4
Bin truncation	3.6	0.3	0.7	8.7	0.2	1.3	4.1	0.3	0.8
MC generator	1.0	1.4	10.2	1.0	1.9	3.2	0.8	2.2	4.0
UE	0.7	0.4	negl.	2.1	0.8	0.3	3.2	1.3	1.0
Total	4.0	2.1	10.5	9.2	3.1	4.5	5.8	3.5	5.4

The uncertainty on the track reconstruction efficiency is estimated to be 3% based on variations of track selection criteria and possible imperfections in the description of the TPC–ITS track matching efficiency in the simulation [16]. Consequently, a new response matrix is constructed after removing 3% of detector-level tracks randomly before jet finding and is used to unfold the measured data in order to estimate the systematic uncertainties on the reported jet observables.

The number of iterations is optimized to a value that minimizes the total uncertainty in unfolded data. As a systematic study, the number of iterations is varied by ± 1 with respect to the default value and the average difference of the modified unfolded distributions from the default one is considered a systematic uncertainty. To estimate the systematic uncertainty due to the change in the shape of the prior distribution,

Table 3: Summary of systematic uncertainties (in %) on dN/dz^{ch} in z^{ch} bins for selected intervals of jet p_T for jet $R = 0.2, 0.3,$ and 0.4 in MB and HM events.

Jet p_T (GeV/c)	Sources	Systematic uncertainties on dN/dz^{ch} for MB (%)								
		$R = 0.2$			$R = 0.3$			$R = 0.4$		
		z^{ch} bin			z^{ch} bin			z^{ch} bin		
		0 – 0.1	0.3 – 0.4	0.9 – 1	0 – 0.1	0.3 – 0.4	0.9 – 1	0 – 0.1	0.3 – 0.4	0.9 – 1
10–20	Track reconst. efficiency	4.4	1.2	4.7	4.6	0.4	6.6	4.5	0.3	8.4
	Unfolding parameter	0.8	0.1	0.1	0.7	0.1	0.2	0.8	0.3	0.1
	Prior change	3.8	0.6	4.7	2.3	2.1	3.1	2.1	2.1	2.3
	Bin truncation	5.4	5.8	16.4	8.9	7.9	22.2	12.2	10.3	27.9
	MC generator	5.1	1.1	11.4	2.2	0.9	9.4	0.6	0.6	8.0
	UE	4.5	0.1	negl.	3.7	0.2	negl.	2.9	0.2	0.1
	Total	10.5	6.1	21.1	11.2	8.2	25.2	13.5	10.5	30.3
60–80	Track reconst. efficiency	3.2	0.8	12.6	3.2	1.5	14.4	3.5	1.7	16.3
	Unfolding parameter	0.3	1.1	1.8	0.4	1.7	3.4	0.4	0.6	0.6
	Prior change	1.4	0.9	6.5	1.8	2.1	17.5	0.4	1.3	3.4
	Bin truncation	0.9	0.5	0.5	0.6	0.4	negl.	0.2	0.5	0.4
	MC generator	0.4	15.4	35.9	10.8	23.6	29.4	16.4	17.5	60.3
	UE	1.7	negl.	negl.	2.9	0.1	negl.	3.3	0.1	negl.
	Total	4.0	15.5	38.6	11.8	23.8	37.3	17.1	17.6	62.6
Jet p_T (GeV/c)	Sources	Systematic uncertainties on dN/dz^{ch} for HM (%)								
		$R = 0.2$			$R = 0.3$			$R = 0.4$		
		z^{ch} bin			z^{ch} bin			z^{ch} bin		
		0 – 0.1	0.3 – 0.4	0.9 – 1	0 – 0.1	0.3 – 0.4	0.9 – 1	0 – 0.1	0.3 – 0.4	0.9 – 1
10–20	Track reconst. efficiency	5.8	0.9	7.3	6.1	0.9	8.8	4.4	1.3	15.7
	Unfolding parameter	0.1	negl.	0.4	0.2	0.1	0.2	0.8	0.2	0.1
	Prior change	0.8	0.9	4.6	negl.	1.1	2.6	1.8	2.0	0.8
	Bin truncation	10.9	7.4	19.0	15.1	10.3	25.7	19.5	14.0	28.7
	MC generator	5.1	1.1	11.4	2.2	0.9	9.4	0.6	0.6	8.0
	UE	0.6	0.1	4.2	0.1	0.1	0.6	0.5	0.1	1.6
	Total	13.4	7.6	24.1	16.4	10.4	28.9	20.1	14.2	33.7
60–80	Track reconst. efficiency	3.5	1.3	4.6	3.9	0.8	3.2	4.2	1.3	16.0
	Unfolding parameter	0.3	0.1	4.4	0.2	0.4	1.3	0.2	0.3	2.5
	Prior change	2.3	0.5	5.4	2.3	0.8	8.8	2.5	0.5	14.0
	Bin truncation	1.5	1.2	0.7	1.3	0.8	0.1	0.9	0.6	0.2
	MC generator	0.4	15.4	35.9	10.8	23.6	29.4	16.4	17.5	60.3
	UE	0.9	negl.	negl.	1.5	0.1	negl.	1.7	0.1	negl.
	Total	4.6	15.5	36.9	11.9	23.6	30.9	17.2	17.6	64.0

the response matrix is reweighted with the ratio between the measured distribution and the one from detector-level MC. The systematic uncertainty is evaluated as the difference between the distributions obtained by unfolding with the default and reweighted response matrices. Additionally, the sensitivity of

Table 4: Summary of systematic uncertainties (in %) on $dN/d\xi^{\text{ch}}$ in ξ^{ch} bins for selected intervals of jet p_T for jet $R = 0.2, 0.3,$ and 0.4 in MB and HM events.

Jet p_T (GeV/c)	Sources	Systematic uncertainties on $dN/d\xi^{\text{ch}}$ for MB (%)								
		$R = 0.2$			$R = 0.3$			$R = 0.4$		
		ξ^{ch} bin			ξ^{ch} bin			ξ^{ch} bin		
		0 – 0.4	2.8 – 3.2	4.8 – 5.2	0 – 0.4	2.8 – 3.2	4.8 – 5.2	0 – 0.4	2.8 – 3.2	4.8 – 5.2
10–20	Track reconst. efficiency	3.1	4.3	5.7	4.4	4.4	20.6	6.0	4.3	18.0
	Unfolding parameter	0.3	0.6	21.5	0.2	0.6	15.0	0.1	0.8	16.6
	Prior change	1.0	3.2	1.5	0.9	2.2	9.8	negl.	0.6	6.9
	Bin truncation	12.7	5.4	1.6	17.2	8.9	13.7	21.7	12.0	28.8
	MC generator	5.3	4.7	28.2	7.2	1.7	13.6	9.2	0.7	9.0
	UE	negl.	1.5	5.6	0.1	1.4	3.8	0.1	0.8	2.8
	Total	14.1	9.1	36.4	19.2	10.4	33.7	24.3	12.8	39.6
60–80	Track reconst. efficiency	7.4	2.9	6.9	8.8	2.8	6.2	9.1	2.7	6.1
	Unfolding parameter	0.4	0.3	1.9	2.3	0.3	0.4	0.4	0.6	1.4
	Prior change	1.9	0.1	13.3	5.2	3.6	15.5	6.5	5.6	12.6
	Bin truncation	0.2	0.3	4.4	negl.	0.1	2.8	0.1	0.1	1.3
	MC generator	20.4	1.8	28.3	18.0	6.8	3.2	15.5	13.4	6.0
	UE	negl.	0.5	0.7	negl.	0.7	1.1	negl.	0.8	1.6
	Total	21.8	3.5	32.4	20.8	8.2	17.3	19.1	14.8	15.4
Jet p_T (GeV/c)	Sources	Systematic uncertainties on $dN/d\xi^{\text{ch}}$ for HM (%)								
		$R = 0.2$			$R = 0.3$			$R = 0.4$		
		ξ^{ch} bin			ξ^{ch} bin			ξ^{ch} bin		
		0 – 0.4	2.8 – 3.2	4.8 – 5.2	0 – 0.4	2.8 – 3.2	4.8 – 5.2	0 – 0.4	2.8 – 3.2	4.8 – 5.2
10–20	Track reconst. efficiency	4.2	8.7	16.3	5.0	5.2	5.8	5.0	3.8	19.9
	Unfolding parameter	0.6	0.2	22.2	1.1	0.1	1.5	1.1	0.7	11.3
	Prior change	0.5	0.6	7.4	1.1	0.2	4.7	2.3	2.3	3.4
	Bin truncation	15.1	10.2	25.2	22.1	14.7	33.6	28.0	18.7	36.6
	MC generator	5.3	4.7	28.2	7.2	1.7	13.6	9.2	0.7	9.0
	UE	negl.	2.0	5.0	0.1	1.8	3.5	0.1	1.1	0.1
	Total	16.6	14.4	47.6	23.8	15.8	37.2	30.0	19.3	44.2
60–80	Track reconst. efficiency	5.9	2.9	5.4	7.3	3.3	6.4	8.0	3.1	6.3
	Unfolding parameter	0.8	0.2	2.1	0.6	0.1	2.2	0.6	negl.	2.1
	Prior change	0.9	2.4	negl.	1.3	2.3	0.2	2.5	2.5	0.1
	Bin truncation	0.3	1.2	3.3	0.2	1.0	2.7	0.2	0.7	1.8
	MC generator	20.4	1.8	28.3	18.0	6.8	3.2	15.5	13.4	6.0
	UE	negl.	0.1	0.3	negl.	negl.	0.4	negl.	0.1	negl.
	Total	21.3	4.3	29.1	19.5	8.0	8.0	17.6	14.0	9.1

the unfolded result to combinatorial jets (a contamination of jets purely comprised of soft particles not correlated with a given hard scattering [72]) is reflected in bin migration effects and the corresponding systematic uncertainty is estimated by varying the lower and upper bounds of detector-level jet p_T by +5

and -20 GeV/ c before the construction of the modified response matrix.

As discussed in Sec. 4.1, the response matrices used to unfold the data are constructed using the information of correspondence between truth- and detector-level jets and their constituents obtained from simulations with the PYTHIA 8 generator. However, the particular structure of jets simulated by one event generator may be different from that in other event generators, which may, in turn, affect the unfolded distributions. To account for the model dependence uncertainty, another MC event generator, EPOS LHC [64], is used to construct a modified response matrix, and the corresponding systematic uncertainty is evaluated from the difference with respect to the default results obtained with PYTHIA 8.

To estimate the systematic uncertainty due to the UE estimation method, the random cone method is applied where two cones are randomly generated with the same pseudorapidity as the leading jet, and with azimuthal angles with respect to the leading jet axis ($\Delta\phi$) within $\pi/3 < \Delta\phi < 2\pi/3$ and $-2\pi/3 < \Delta\phi < -\pi/3$, instead of using a fixed azimuthal angle of $\Delta\phi = \pi/2$ as done in the perpendicular cone method. Similarly to the approach adopted in the perpendicular cone method, the UE contributions to the jet observables are estimated using the information of particles from the two random cones and are provided as input to construct the modified response matrices. The difference between the unfolded distributions obtained for the two UE estimation methods is reported as the corresponding systematic uncertainty.

Table 2 summarizes the estimated systematic uncertainties on $\langle N_{\text{ch}} \rangle$ from the different sources in MB and HM events. Similarly, the systematic uncertainties on z^{ch} and ξ^{ch} distributions in MB and HM events are outlined in Tables 3 and 4, respectively. In most of the cases, the uncertainties due to track reconstruction efficiency and model dependence turn out to be the dominant sources of systematic uncertainties.

6 Results

6.1 Mean charged-particle multiplicity in the leading jet $\langle N_{\text{ch}} \rangle$

Figure 1 shows the mean number of charged particles within leading jets as a function of jet p_{T} in pp collisions at $\sqrt{s} = 13$ TeV for MB (top) and HM (bottom) events. The upper panels show the corrected $\langle N_{\text{ch}} \rangle$ distributions for jet $R = 0.2$ (left), 0.3 (middle), and 0.4 (right) in the pseudorapidity ranges $|\eta_{\text{jet}}| < (0.9 - R)$. The data points and the corresponding systematic uncertainties are presented by solid markers and shaded bands, respectively. The statistical uncertainties are represented by vertical error bars (smaller than the marker size). Results are compared to predictions from PYTHIA 8 denoted by open markers. The lower panels show the ratio between PYTHIA 8 predictions and data. A monotonic increment of $\langle N_{\text{ch}} \rangle$ is observed with increasing jet p_{T} as well as with jet radius R for both MB and HM events. The slope of increment at low jet p_{T} is larger than that at high jet p_{T} indicating that as p_{T} increases, more momentum is carried by single constituents. The measured trend is very well captured by PYTHIA 8 within the systematic uncertainties.

The top panels of Fig. 2 show the ratios of $\langle N_{\text{ch}} \rangle$ between HM and MB events as a function of jet p_{T} in comparison to predictions from PYTHIA 8. The data points are shown by solid markers and the PYTHIA 8 predictions are represented by open markers for jet $R = 0.2$ (left), 0.3 (middle), and 0.4 (right). The ratios between PYTHIA 8 predictions and data are shown in the bottom panels. A mild increase in the mean number of jet constituents is observed in HM compared to that in MB event class. The magnitude of the increment is found to decrease gradually with increasing jet p_{T} . A maximum increment of $\sim 10\%$ (8% , 6%) for jet $R = 0.2$ (0.3 , 0.4) is observed towards low jet p_{T} while there is no increment at high jet p_{T} for all R . PYTHIA 8 qualitatively reproduces the data, however, fails to quantitatively reproduce the jet- p_{T} dependence. This observation indicates a softening of jet constituents in HM events compared to MB for low- p_{T} jets, which aligns with the CMS measurement of a complementary observable, namely the mean p_{T} of jet constituents, in pp collisions at $\sqrt{s} = 7$ TeV [73].

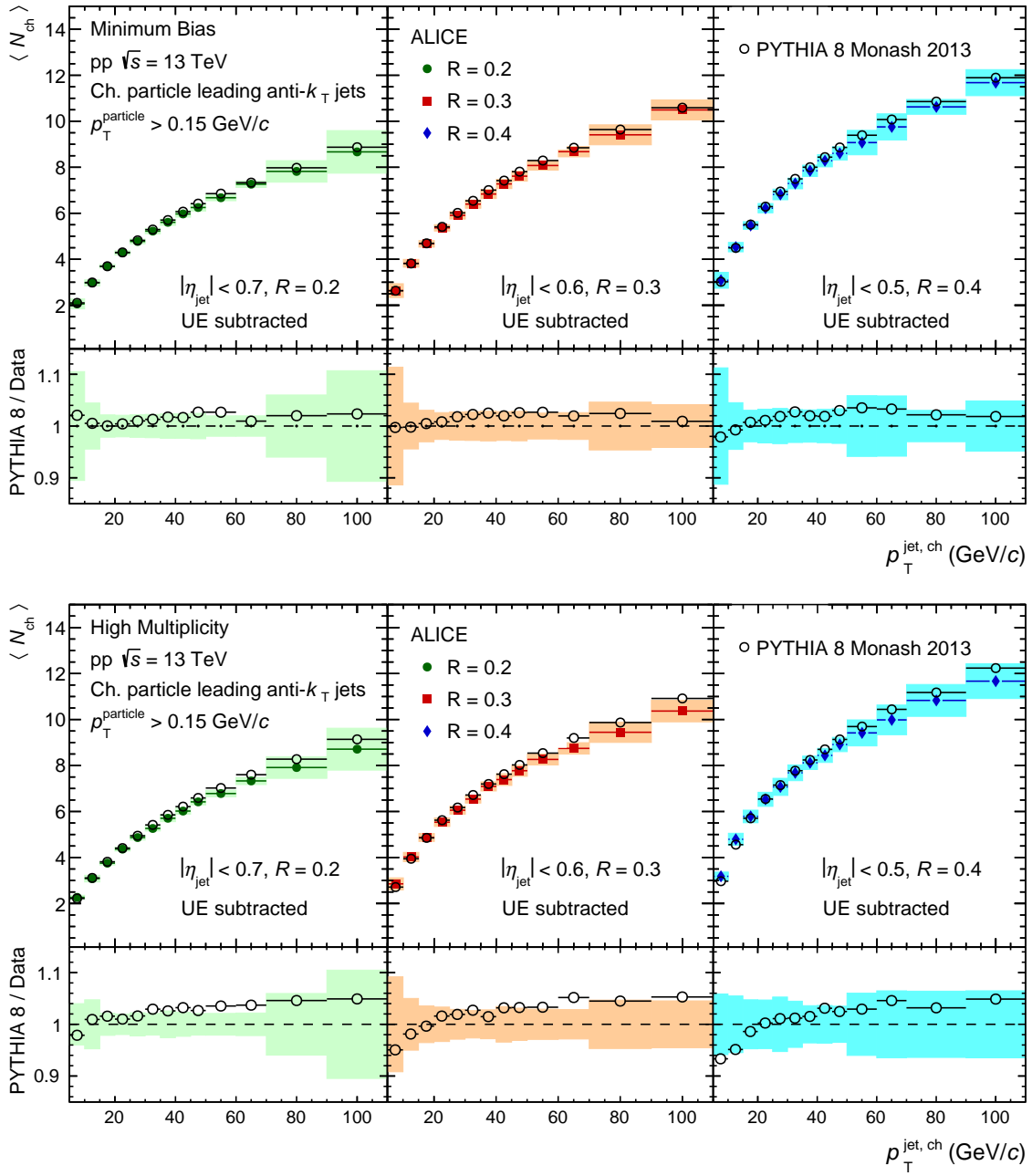


Figure 1: $\langle N_{ch} \rangle$ as a function of leading jet p_T for MB (top) and HM (bottom) events for jet radii $R = 0.2$ (left), 0.3 (middle), and 0.4 (right). The distributions are compared with PYTHIA 8 predictions.

6.2 Jet fragmentation

6.2.1 z^{ch}

Figure 3 shows the jet fragmentation function z^{ch} for jet radii 0.2 (left), 0.3 (middle), and 0.4 (right) within the jet- p_T intervals $10\text{--}20$ GeV/c, $20\text{--}30$ GeV/c, $30\text{--}40$ GeV/c, $40\text{--}60$ GeV/c, and $60\text{--}80$ GeV/c for both MB (top) and HM (bottom) events. The solid markers represent the corrected results in the different jet- p_T intervals and the shaded bands are the corresponding systematic uncertainties. The statistical uncertainties are represented by vertical error bars (mostly smaller than the marker size). The distributions in different jet- p_T intervals are consistent within systematic uncertainties for wider jets ($R = 0.4$) in HM (MB) events, in the range $0.1 < z^{ch} < 1$ ($0.1 < z^{ch} < 0.9$), indicating jet- p_T independent frag-

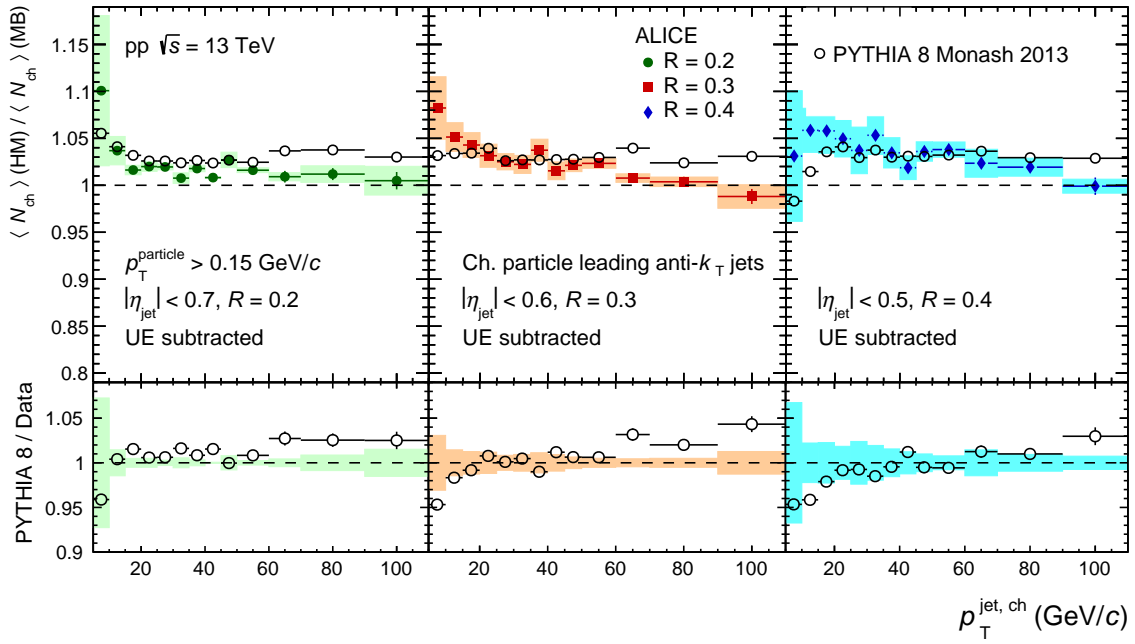


Figure 2: Top panel: The ratio of $\langle N_{ch} \rangle$ between HM and MB events for jet radii $R = 0.2$ (left), 0.3 (middle), and 0.4 (right) compared to PYTHIA 8 predictions. Bottom panel: Ratio between PYTHIA 8 predictions and the measured values.

mentation function. However, for narrower jets ($R = 0.2$ and 0.3), the fragmentation functions depend on jet p_T in both MB and HM events.

In Fig. 4, the measured fragmentation functions are compared to predictions obtained from PYTHIA 8 and EPOS LHC event generators for MB events (top) and with PYTHIA 8 predictions for HM events (bottom). For MB events, in the lowest and highest jet- p_T intervals (10 – 20 and 60 – 80 GeV/ c), PYTHIA 8 describes the data within systematic uncertainties; however, it underestimates the data in the intermediate jet- p_T intervals (20 – 30 , 30 – 40 , and 40 – 60 GeV/ c) and intermediate z^{ch} values ($0.5 < z^{ch} < 0.7$). EPOS LHC, on the other hand, reproduces the data better compared to PYTHIA 8 for the jet- p_T intervals 10 – 20 , 20 – 30 , 30 – 40 , and 40 – 60 GeV/ c . For HM events, the ratios between the PYTHIA 8 predictions and data in the measured jet- p_T intervals for all the jet R show similar trends as observed in MB results.

Figure 5 depicts the ratios of z^{ch} distributions between HM and MB events for three jet- p_T intervals, 10 – 20 GeV/ c (top), 30 – 40 GeV/ c (middle), and 60 – 80 GeV/ c (bottom) and for jet $R = 0.2$ (left), 0.3 (middle), and 0.4 (right). Comparisons with the PYTHIA 8 predictions (denoted by open markers) are also shown. The distribution of z^{ch} in HM events is noticeably different from that from MB events for low- p_T jets (10 – 20 GeV/ c), as shown in the ratio plots in the top panels of Fig. 5. The fragmentation probability of particles at low (high) z^{ch} is found to be enhanced (suppressed) in HM events compared to that in MB. This effect becomes more pronounced with increasing jet radius at a given jet p_T . The trend becomes less pronounced at higher jet p_T as it can be seen in the middle and bottom panels of Fig. 5. PYTHIA 8 qualitatively reproduces the data except at high z^{ch} (> 0.7) for jet $p_T = 60$ – 80 GeV/ c and jet $R = 0.4$, where the statistical and systematic uncertainties are large.

A recent ALICE measurement of semi-inclusive azimuthal distributions of charged-particle jets recoiling from a high- p_T hadron trigger also shows significant azimuthal broadening in HM events compared to those in MB events and PYTHIA 8 follows a similar broadening [57]. A detailed investigation revealed that the HM event selection based on the V0 detector at forward rapidity introduces a bias towards multi-jet topologies, thereby affecting the azimuthal distribution. However, the measurement of intra-jet properties may evade the complication of multi-jet bias since it focuses on modifications within the lead-

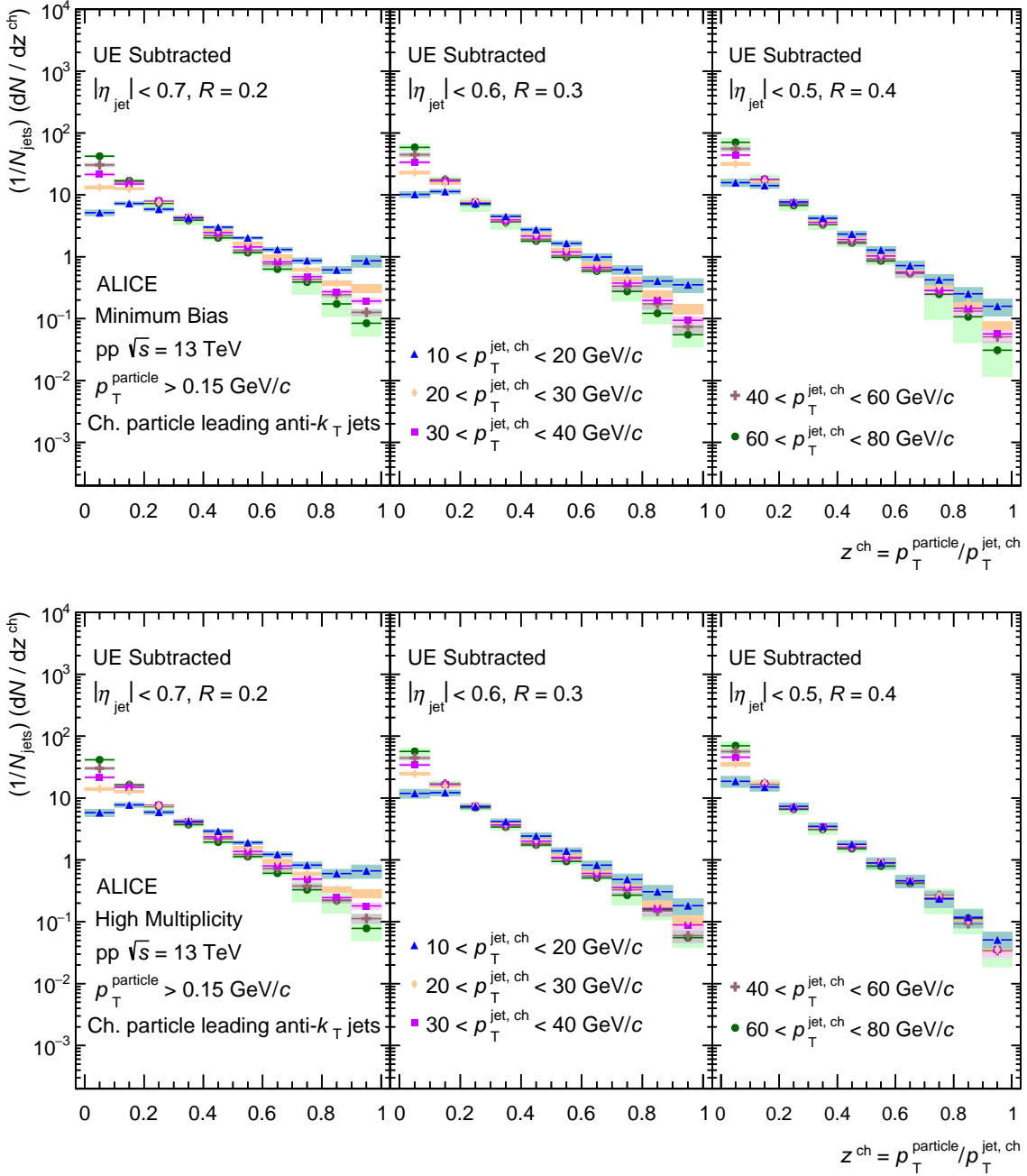


Figure 3: z^{ch} distributions in leading jets for different jet z^{ch} transverse momenta in MB (top) and HM (bottom) events for jet $R = 0.2$ (left), 0.3 (middle), and 0.4 (right).

ing jet, which, to first order, is independent of other jets in the event. By measuring intra-jet properties rather than jet correlations, the results shown in Fig. 5, therefore, provide complementary constraints on jet modification in small systems. A further investigation using less biased HM events (selected based on the total charged-particle multiplicity) in PYTHIA 8 shows a similar modification of the jet fragmentation function z^{ch} , hinting towards possible sources other than QGP formation, that may contribute to the observed modification.

From a theoretical perspective, several efforts [74–76] have been made to understand the jet modification in high-multiplicity events compared to minimum-bias ones in pp collisions. In Ref. [76], a modification of jet properties in HM compared to MB events is predicted in pp collisions due to phenomena such as multiparton interactions (MPI) with color reconnection (CR) in PYTHIA 8 as well as enhancement in the

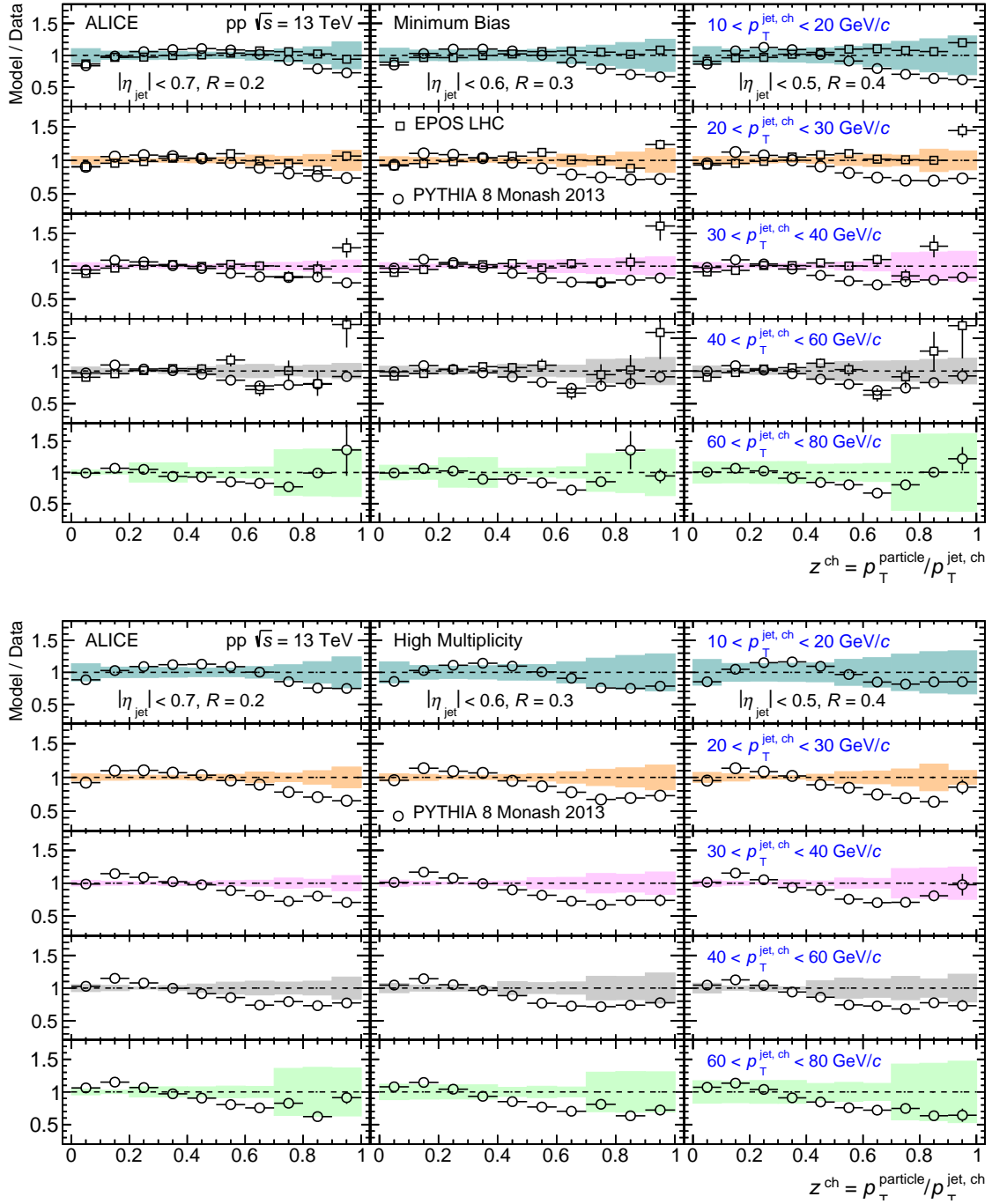


Figure 4: Top: Ratios of PYTHIA 8 and EPOS LHC predictions to data for z^{ch} distributions in different $p_{\text{T}}^{\text{jet, ch}}$ intervals in MB events for jet $R = 0.2$ (left), 0.3 (middle), and 0.4 (right). Bottom: Ratios of PYTHIA 8 predictions to data for z^{ch} distributions in different $p_{\text{T}}^{\text{jet, ch}}$ intervals in HM events for jet $R = 0.2$ (left), 0.3 (middle), and 0.4 (right).

number of gluon-initiated jets in high-multiplicity events compared to that in minimum-bias collisions.

Using similar conditions for selecting MB and HM events and other kinematic selections as applied to data, the observed behavior in the ratio of z^{ch} distributions between HM and MB events in PYTHIA 8 is further investigated for $10 < p_{\text{T}}^{\text{jet, ch}} < 20$ GeV/c and jet radius 0.4 . Two event samples with configurations ‘MPI: ON, CR: ON’ (default setting in PYTHIA 8) and ‘MPI: OFF, CR: OFF’ (where both MPI

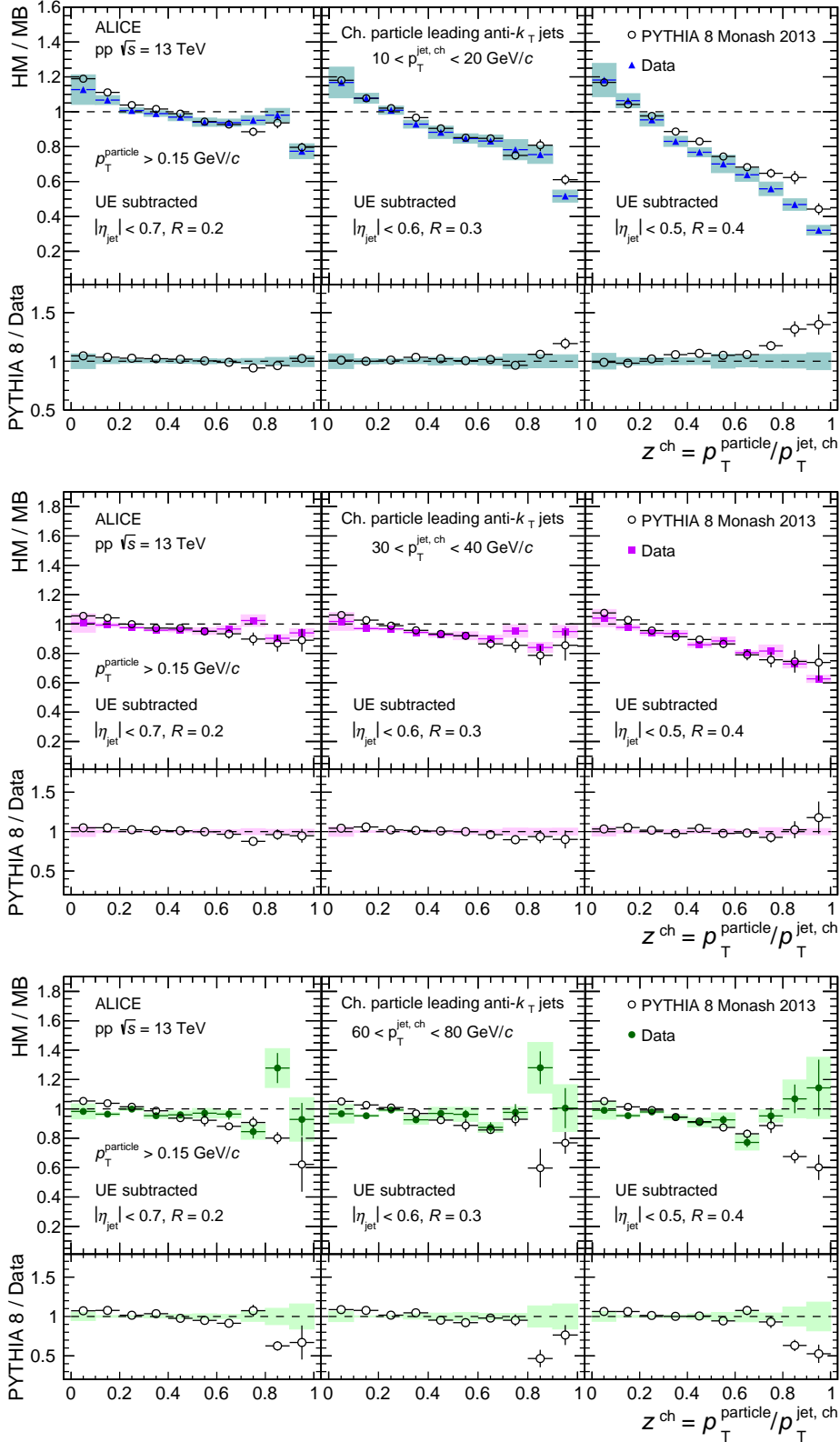


Figure 5: The ratio between HM and MB distributions of z^{ch} for $p_T^{\text{jet, ch}}$ intervals 10–20 GeV/c (top), 30–40 GeV/c (middle), and 60–80 GeV/c (bottom) for jet $R = 0.2$ (left), 0.3 (middle), and 0.4 (right).

and CR are switched off) are generated using PYTHIA 8 for minimum-bias and high-multiplicity pp collisions at $\sqrt{s} = 13$ TeV. Figure 6 (left) shows the comparison of z^{ch} distributions for inclusive (quark- and

gluon-initiated) leading charged-particle jets in the interval $10 < p_T^{\text{jet, ch}} < 20$ GeV/c between HM (blue circles) and MB (red boxes) events for the above-mentioned configurations. The ratio of z^{ch} distributions between HM and MB events (bottom panel) shows a significant modification of jet fragmentation in the presence of MPI with CR and the magnitude of the modification gets reduced when MPI and CR are switched off, indicating the dependence of jet modification on MPI and CR. The origin of the residual amount of modification in the absence of both MPI and CR is further investigated using gluon-initiated jets to check the dependence of jet modification on the nature of the initiating parton. A geometrical matching procedure based on the closest-distance approach (as applied in Ref. [76]) is followed to match hard-scattered partons with the leading jets. The fraction of gluon-initiated jets is found to be larger in HM events ($\sim 83\%$) than in MB events ($\sim 77\%$). Figure 6 (right) shows the comparison of z^{ch} distributions for gluon-initiated leading charged-particle jets between HM (blue circles) and MB (red boxes) events for ‘MPI: OFF, CR: OFF’ configuration, showing a further, even though small, reduction of the modification with increasing multiplicity as compared to the case of inclusive jets. These observations indicate that MPI with CR and enhanced gluonic contribution are playing major roles in the change of jet fragmentation in high-multiplicity events compared to minimum-bias events.

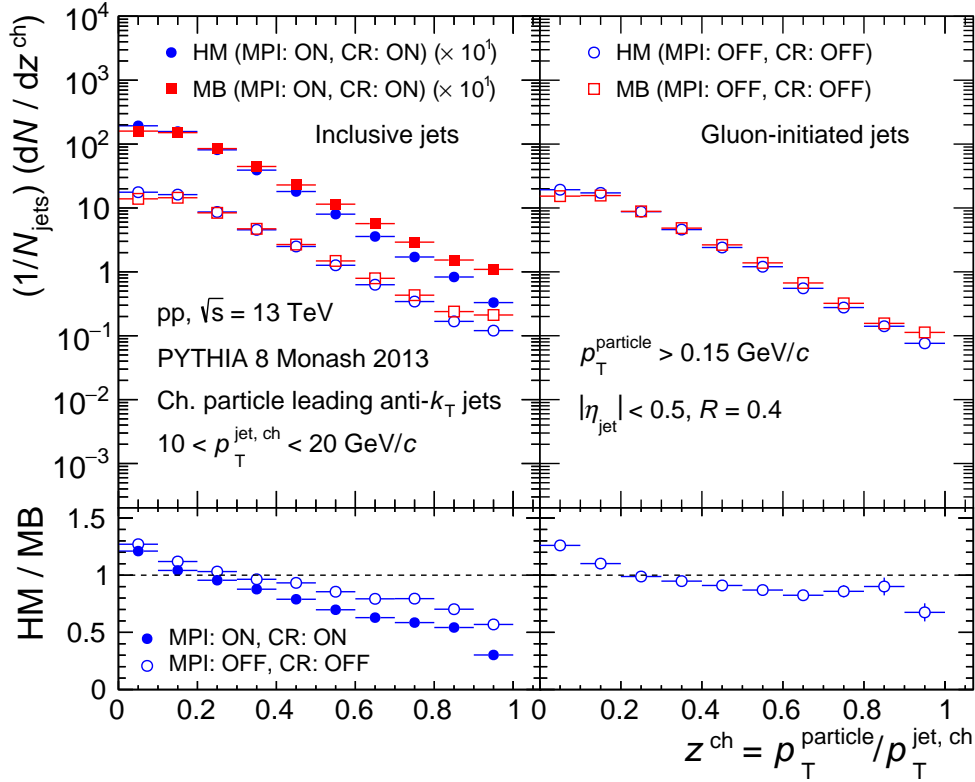


Figure 6: Top panel: Distributions of z^{ch} for the jet- p_T interval 10–20 GeV/c for inclusive (quark- and gluon-initiated) jets with ‘MPI: ON, CR: ON’ and ‘MPI: OFF, CR: OFF’ configurations (left), and for gluon-initiated jets with ‘MPI: OFF, CR: OFF’ configuration (right) using PYTHIA 8. Bottom panel: Ratio of z^{ch} distributions between HM and MB events.

6.2.2 ξ^{ch}

Figure 7 shows the jet fragmentation function ξ^{ch} for jet $R = 0.2$ (left), 0.3 (middle), and 0.4 (right) within the jet- p_T intervals 10–20, 20–30, 30–40, 40–60, and 60–80 GeV/c for both MB (top) and HM (bottom) events. The solid markers represent the corrected results in different jet- p_T intervals and the shaded bands

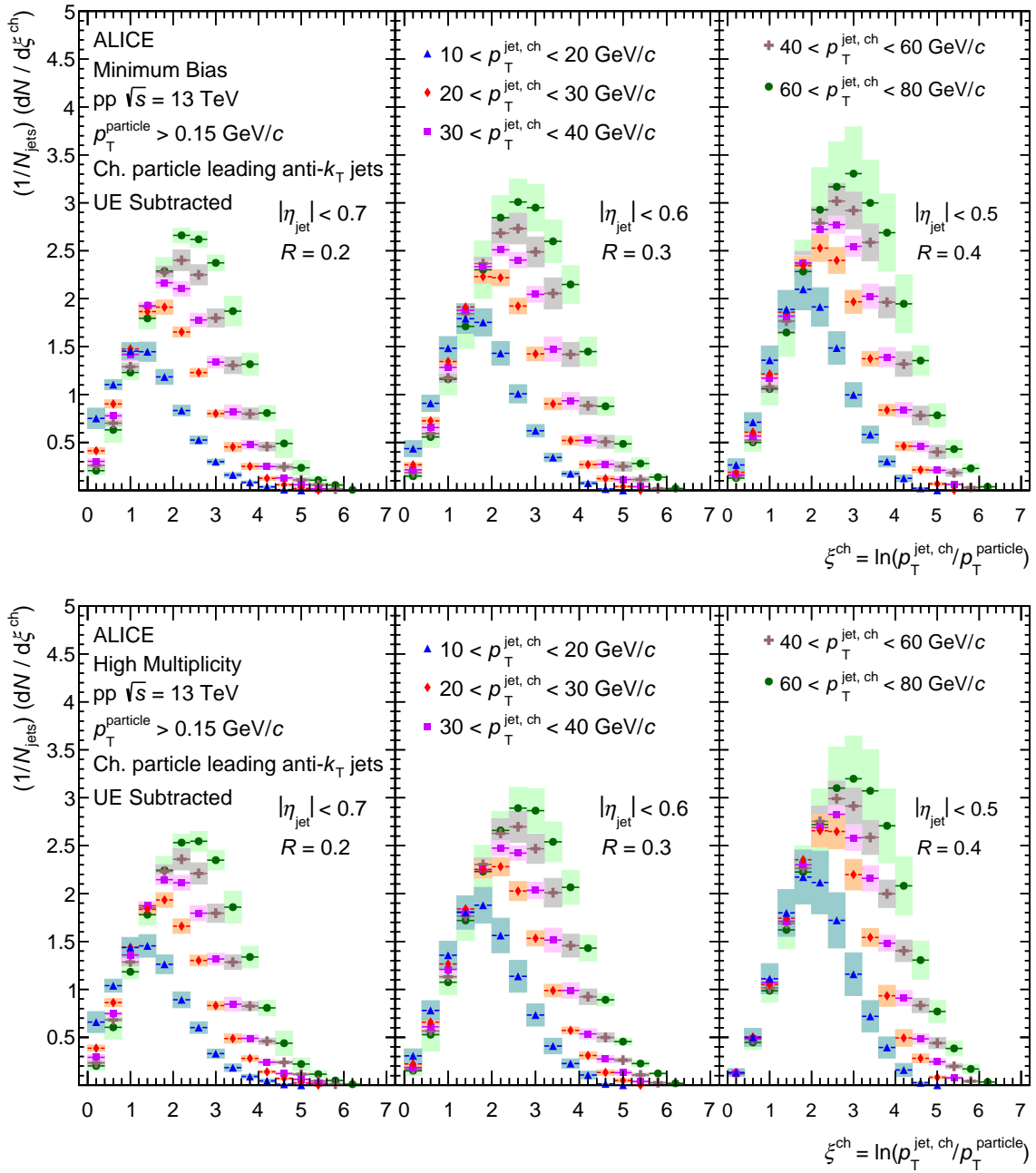


Figure 7: ξ^{ch} distributions in leading jets for different jet p_{T} transverse momenta in MB (top) and HM (bottom) events for jet $R = 0.2$ (left), 0.3 (middle), and 0.4 (right).

are the corresponding systematic uncertainties. The statistical uncertainties are represented by vertical error bars (mostly smaller than the marker size). Jet- p_{T} independent ξ^{ch} distributions are observed for $\xi^{\text{ch}} < 2$ and jet $R = 0.4$ in both MB and HM events, while the ξ^{ch} distributions are found to depend on jet p_{T} for jet $R = 0.2$ and 0.3 . These observations are complementary to those observed in z^{ch} distributions. In addition, a pronounced peak structure, commonly known as a “hump-backed plateau” is observed, resulting from the suppression of low- p_{T} particle production predicted by QCD coherence [40, 68]. With increasing jet p_{T} and rising jet R , the area of the ξ^{ch} distributions increases, complementing the results obtained from $\langle N_{\text{ch}} \rangle$, indicating an increase of charged-particle multiplicity in jets with increasing jet p_{T} . These results show similar trends as the previous ALICE measurement in pp collisions at $\sqrt{s} = 7$ TeV [13].

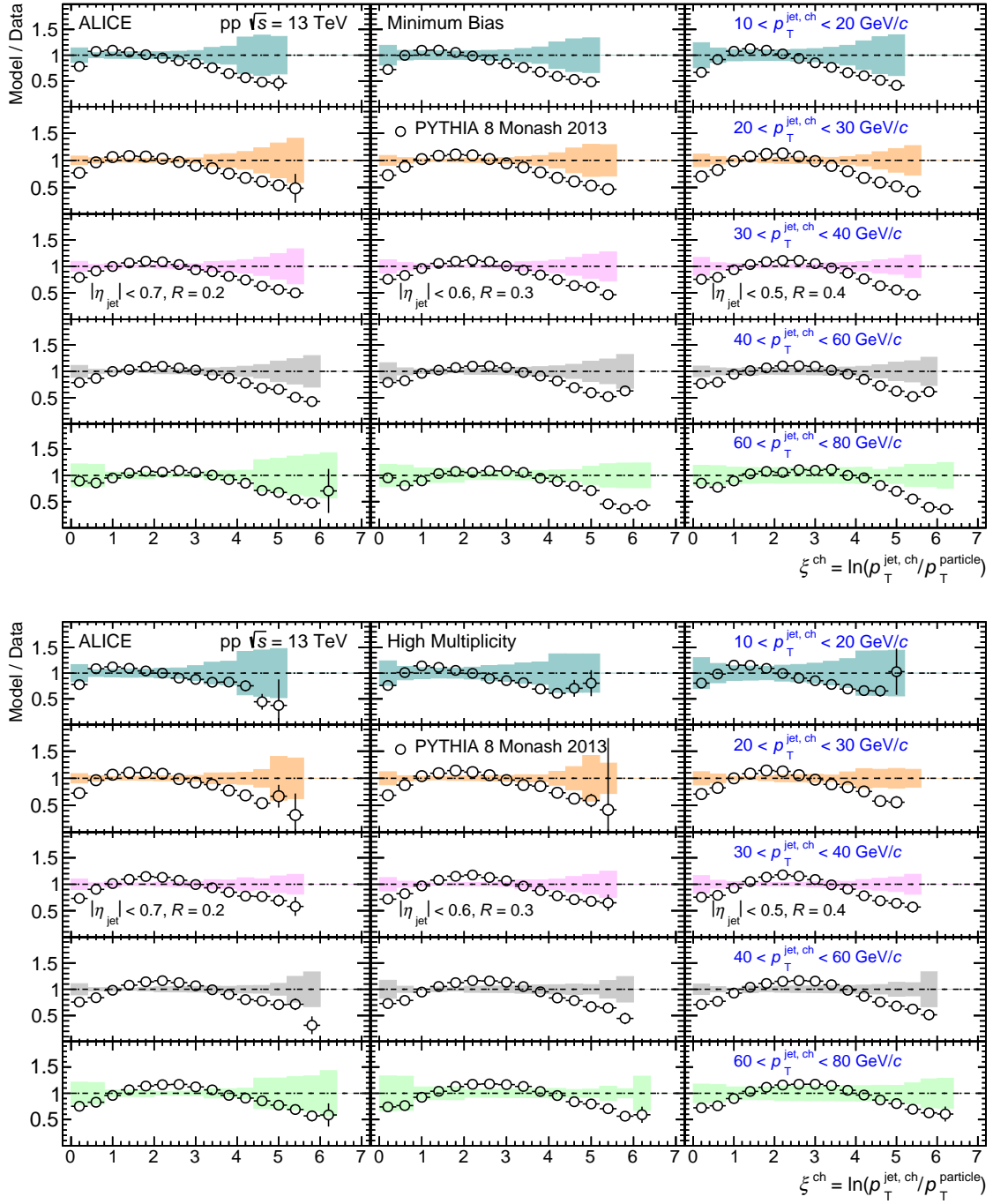


Figure 8: Ratios of PYTHIA 8 predictions to data for ξ^{ch} distributions in different $p_T^{\text{jet, ch}}$ intervals in MB (top) and HM (bottom) events for jet $R = 0.2$ (left), 0.3 (middle), and 0.4 (right).

The comparisons of ξ^{ch} distributions with PYTHIA 8 predictions are shown in Fig. 8. It can be seen that PYTHIA 8 qualitatively reproduces the data for both MB and HM events, similarly to what is found for the z^{ch} distributions. Figure 9 shows the ratio of ξ^{ch} distributions between HM and MB events for three jet- p_T ranges, 10–20 GeV/c (top), 30–40 GeV/c (middle), and 60–80 GeV/c (bottom) and for three jet $R = 0.2$ (left), 0.3 (middle), and 0.4 (right). A clear suppression of ξ^{ch} distribution at low- ξ^{ch} values is observed in HM events compared to MB events in the lowest (10–20 GeV/c) jet- p_T interval for $R = 0.4$. The amount of this suppression gets reduced with decreasing jet R at a fixed jet p_T and decreases with increasing jet p_T at a given jet radius. These observations are complementary to the results as a function

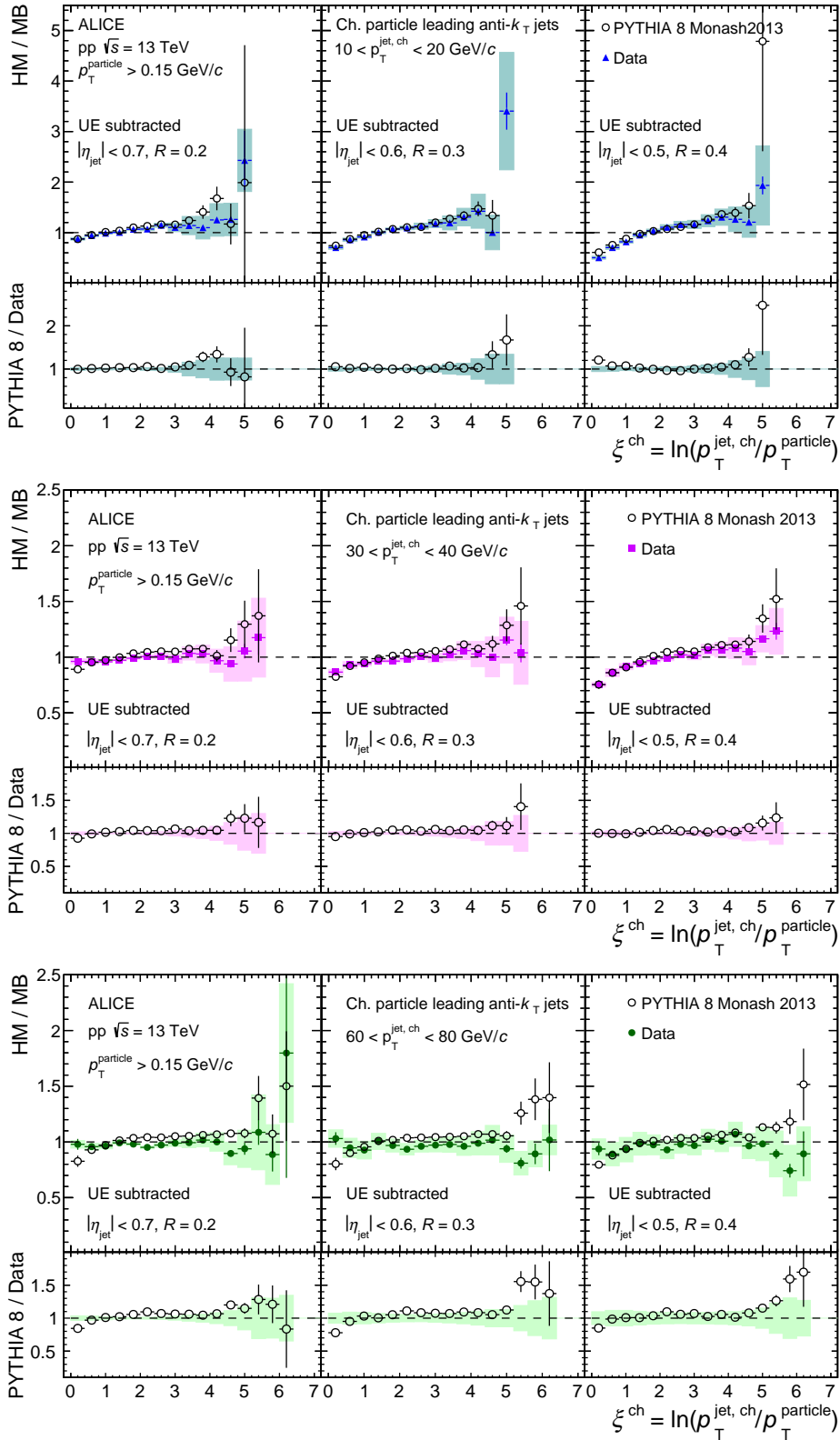


Figure 9: The ratio between HM and MB distributions of ξ^{ch} for $p_{\text{T}}^{\text{jet, ch}}$ intervals 10–20 GeV/c (top), 30–40 GeV/c (middle), and 60–80 GeV/c (bottom) for jet $R = 0.2$ (left), 0.3 (middle), and 0.4 (right).

of z^{ch} reported above and the trends are well reproduced by PYTHIA 8.

7 Summary

In summary, this work reports the measurement of multiplicity-dependent charged-particle intra-jet properties of leading jets in pp collisions at $\sqrt{s} = 13$ TeV using the ALICE detector at the LHC. The mean charged-particle multiplicity $\langle N_{\text{ch}} \rangle$ and jet fragmentation functions z^{ch} and ξ^{ch} for leading jets are measured for minimum-bias and high-multiplicity events using the anti- k_{T} jet finding algorithm with $R = 0.2, 0.3,$ and 0.4 . A monotonic increase in $\langle N_{\text{ch}} \rangle$ is observed in both MB and HM events as a function of jet p_{T} as well as with increasing jet radius R . It is found to be slightly larger in high-multiplicity events in comparison with minimum-bias ones; PYTHIA 8 also exhibits a similar pattern. A jet- p_{T} independent jet fragmentation is observed in both MB and HM events within certain ranges of z^{ch} and ξ^{ch} values only for wider jets ($R = 0.4$). EPOS LHC reproduces the z^{ch} distributions better than PYTHIA 8 in MB events. The observed ‘‘hump-backed plateau’’ structure in ξ^{ch} distributions originates from the suppression of low- p_{T} particle production predicted by QCD coherence. The ξ^{ch} distributions for both MB and HM events are qualitatively reproduced by PYTHIA 8.

The fragmentation functions in HM events are noticeably different from those in MB events. The probability of jet fragmentation into particles with low z^{ch} gets enhanced, followed by a suppression of high- z^{ch} particles in HM events compared to that in MB. The observed jet modification is more prominent for low- p_{T} jets ($10\text{--}20$ GeV/ c) with larger jet radius ($R = 0.4$) and is reduced with increasing jet p_{T} at a given radius. These trends are qualitatively reproduced by PYTHIA 8. Similar conclusions are obtained when studying the fragmentation function in MB and HM events using the ξ^{ch} variable.

Recently, a selection bias towards multi-jet topology has been argued to affect the observed azimuthal broadening in the sample of high-multiplicity events defined from the V0M signal amplitudes. The modifications of intra-jet properties for leading jets are independent of the presence of other jets in an event and are therefore less prone to such biases. An investigation using PYTHIA 8 with a less biased HM event selection also shows a similar amount of modification. A detailed study using PYTHIA 8 shows that the major sources of the modification in jet fragmentation are multiparton interactions with color reconnection and the enhanced number of gluon-initiated jets in HM events. One can conclude from here that jet modification is observed in small systems with increasing multiplicity, shifting the question towards how one can attribute the observed modification to different causes, e.g., multiparton interactions, jet bias from HM event selection or jet quenching in mini-QGP. Since PYTHIA 8 captures most of the features of the data, the measured modifications cannot be directly interpreted as due to the formation of a QGP in high-multiplicity pp collisions. The measurements of intra-jet properties reported in this work provide new constraints to mechanisms underlying jet modification in small systems.

Acknowledgements

The ALICE Collaboration would like to thank all its engineers and technicians for their invaluable contributions to the construction of the experiment and the CERN accelerator teams for the outstanding performance of the LHC complex. The ALICE Collaboration gratefully acknowledges the resources and support provided by all Grid centres and the Worldwide LHC Computing Grid (WLCG) collaboration. The ALICE Collaboration acknowledges the following funding agencies for their support in building and running the ALICE detector: A. I. Alikhanyan National Science Laboratory (Yerevan Physics Institute) Foundation (ANSL), State Committee of Science and World Federation of Scientists (WFS), Armenia; Austrian Academy of Sciences, Austrian Science Fund (FWF): [M 2467-N36] and Nationalstiftung für Forschung, Technologie und Entwicklung, Austria; Ministry of Communications and High Technologies, National Nuclear Research Center, Azerbaijan; Conselho Nacional de Desenvolvimento Científico e Tecnológico (CNPq), Financiadora de Estudos e Projetos (Finep), Fundação de Amparo à Pesquisa do Estado de São Paulo (FAPESP) and Universidade Federal do Rio Grande do Sul (UFRGS), Brazil; Bulgarian Ministry of Education and Science, within the National Roadmap for Research Infras-

tructures 2020-2027 (object CERN), Bulgaria; Ministry of Education of China (MOEC), Ministry of Science & Technology of China (MSTC) and National Natural Science Foundation of China (NSFC), China; Ministry of Science and Education and Croatian Science Foundation, Croatia; Centro de Aplicaciones Tecnológicas y Desarrollo Nuclear (CEADEN), Cubaenergía, Cuba; Ministry of Education, Youth and Sports of the Czech Republic, Czech Republic; The Danish Council for Independent Research | Natural Sciences, the VILLUM FONDEN and Danish National Research Foundation (DNRF), Denmark; Helsinki Institute of Physics (HIP), Finland; Commissariat à l’Energie Atomique (CEA) and Institut National de Physique Nucléaire et de Physique des Particules (IN2P3) and Centre National de la Recherche Scientifique (CNRS), France; Bundesministerium für Bildung und Forschung (BMBF) and GSI Helmholtzzentrum für Schwerionenforschung GmbH, Germany; General Secretariat for Research and Technology, Ministry of Education, Research and Religions, Greece; National Research, Development and Innovation Office, Hungary; Department of Atomic Energy Government of India (DAE), Department of Science and Technology, Government of India (DST), University Grants Commission, Government of India (UGC) and Council of Scientific and Industrial Research (CSIR), India; National Research and Innovation Agency - BRIN, Indonesia; Istituto Nazionale di Fisica Nucleare (INFN), Italy; Japanese Ministry of Education, Culture, Sports, Science and Technology (MEXT) and Japan Society for the Promotion of Science (JSPS) KAKENHI, Japan; Consejo Nacional de Ciencia (CONACYT) y Tecnología, through Fondo de Cooperación Internacional en Ciencia y Tecnología (FONCICYT) and Dirección General de Asuntos del Personal Académico (DGAPA), Mexico; Nederlandse Organisatie voor Wetenschappelijk Onderzoek (NWO), Netherlands; The Research Council of Norway, Norway; Commission on Science and Technology for Sustainable Development in the South (COMSATS), Pakistan; Pontificia Universidad Católica del Perú, Peru; Ministry of Education and Science, National Science Centre and WUT ID-UB, Poland; Korea Institute of Science and Technology Information and National Research Foundation of Korea (NRF), Republic of Korea; Ministry of Education and Scientific Research, Institute of Atomic Physics, Ministry of Research and Innovation and Institute of Atomic Physics and Universitatea Nationala de Stiinta si Tehnologie Politehnica Bucuresti, Romania; Ministry of Education, Science, Research and Sport of the Slovak Republic, Slovakia; National Research Foundation of South Africa, South Africa; Swedish Research Council (VR) and Knut & Alice Wallenberg Foundation (KAW), Sweden; European Organization for Nuclear Research, Switzerland; Suranaree University of Technology (SUT), National Science and Technology Development Agency (NSTDA) and National Science, Research and Innovation Fund (NSRF via PMU-B B05F650021), Thailand; National Academy of Sciences of Ukraine, Ukraine; Science and Technology Facilities Council (STFC), United Kingdom; National Science Foundation of the United States of America (NSF) and United States Department of Energy, Office of Nuclear Physics (DOE NP), United States of America. In addition, individual groups or members have received support from: European Research Council, Strong 2020 - Horizon 2020 (grant nos. 950692, 824093), European Union; Academy of Finland (Center of Excellence in Quark Matter) (grant nos. 346327, 346328), Finland.

References

- [1] F. Wilczek, “Quantum field theory”, *Rev. Mod. Phys.* **71** (1999) S85–S95, arXiv:hep-th/9803075.
- [2] N. Cabibbo and G. Parisi, “Exponential Hadronic Spectrum and Quark Liberation”, *Phys. Lett. B* **59** (1975) 67–69.
- [3] E. V. Shuryak, “Theory of Hadronic Plasma”, *Sov. Phys. JETP* **47** (1978) 212–219.
- [4] **HotQCD** Collaboration, A. Bazavov *et al.*, “Equation of state in (2+1)-flavor QCD”, *Phys. Rev. D* **90** (2014) 094503, arXiv:1407.6387 [hep-lat].

- [5] **ALICE** Collaboration, “The ALICE experiment – A journey through QCD”, arXiv:2211.04384 [nucl-ex].
- [6] M. Gyulassy and M. Plumer, “Jet Quenching in Dense Matter”, *Phys. Lett. B* **243** (1990) 432–438.
- [7] G.-Y. Qin and X.-N. Wang, “Jet quenching in high-energy heavy-ion collisions”, *Int. J. Mod. Phys. E* **24** (2015) 1530014, arXiv:1511.00790 [hep-ph].
- [8] **JET** Collaboration, K. M. Burke *et al.*, “Extracting the jet transport coefficient from jet quenching in high-energy heavy-ion collisions”, *Phys. Rev. C* **90** (2014) 014909, arXiv:1312.5003 [nucl-th].
- [9] **JETSCAPE** Collaboration, A. Kumar *et al.*, “Inclusive jet and hadron suppression in a multistage approach”, *Phys. Rev. C* **107** (2023) 034911, arXiv:2204.01163 [hep-ph].
- [10] **STAR** Collaboration, M. S. Abdallah *et al.*, “Differential measurements of jet substructure and partonic energy loss in Au+Au collisions at $\sqrt{s_{NN}} = 200$ GeV”, *Phys. Rev. C* **105** (2022) 044906, arXiv:2109.09793 [nucl-ex].
- [11] X.-N. Wang, “QGP and modified jet fragmentation”, *Eur. Phys. J. C* **43** (2005) 223–231, arXiv:nucl-th/0510043.
- [12] K. C. Zapp, F. Krauss, and U. A. Wiedemann, “A perturbative framework for jet quenching”, *JHEP* **03** (2013) 080, arXiv:1212.1599 [hep-ph].
- [13] **ALICE** Collaboration, B. B. Abelev *et al.*, “Charged jet cross sections and properties in proton-proton collisions at $\sqrt{s} = 7$ TeV”, *Phys. Rev. D* **91** (2015) 112012, arXiv:1411.4969 [nucl-ex].
- [14] **ALICE** Collaboration, S. Acharya *et al.*, “Charged jet cross section and fragmentation in proton-proton collisions at $\sqrt{s} = 7$ TeV”, *Phys. Rev. D* **99** (2019) 012016, arXiv:1809.03232 [nucl-ex].
- [15] **ALICE** Collaboration, S. Acharya *et al.*, “Measurements of inclusive jet spectra in pp and central Pb–Pb collisions at $\sqrt{s_{NN}} = 5.02$ TeV”, *Phys. Rev. C* **101** (2020) 034911, arXiv:1909.09718 [nucl-ex].
- [16] **ALICE** Collaboration, S. Acharya *et al.*, “Measurement of charged jet cross section in pp collisions at $\sqrt{s} = 5.02$ TeV”, *Phys. Rev. D* **100** (2019) 092004, arXiv:1905.02536 [nucl-ex].
- [17] **ATLAS** Collaboration, M. Aaboud *et al.*, “Measurement of inclusive jet and dijet cross-sections in proton-proton collisions at $\sqrt{s} = 13$ TeV with the ATLAS detector”, *JHEP* **05** (2018) 195, arXiv:1711.02692 [hep-ex].
- [18] S. K. Prasad, V. Roy, S. Chattopadhyay, and A. K. Chaudhuri, “Elliptic flow (v_2) in pp collisions at energies available at the CERN Large Hadron Collider: A hydrodynamical approach”, *Phys. Rev. C* **82** (2010) 024909, arXiv:0910.4844 [nucl-th].
- [19] P. Ghosh, S. Muhuri, J. K. Nayak, and R. Varma, “Indication of transverse radial flow in high-multiplicity proton–proton collisions at the Large Hadron Collider”, *J. Phys. G* **41** (2014) 035106, arXiv:1402.6813 [hep-ph].
- [20] D. d’Enterria, G. K. Eyyubova, V. L. Korotkikh, I. P. Lokhtin, S. V. Petrushanko, L. I. Sarycheva, and A. M. Snigirev, “Estimates of hadron azimuthal anisotropy from multiparton interactions in proton-proton collisions at $\sqrt{s} = 14$ TeV”, *Eur. Phys. J. C* **66** (2010) 173–185, arXiv:0910.3029 [hep-ph].

- [21] K. Werner, I. Karpenko, and T. Pierog, “The ‘Ridge’ in Proton-Proton Scattering at 7 TeV”, *Phys. Rev. Lett.* **106** (2011) 122004, arXiv:1011.0375 [hep-ph].
- [22] A. Ortiz Velasquez, P. Christiansen, E. Cuautle Flores, I. Maldonado Cervantes, and G. Paic, “Color Reconnection and Flowlike Patterns in pp Collisions”, *Phys. Rev. Lett.* **111** (2013) 042001, arXiv:1303.6326 [hep-ph].
- [23] A. Ortiz, G. Bencedi, and H. Bello, “Revealing the source of the radial flow patterns in proton–proton collisions using hard probes”, *J. Phys. G* **44** (2017) 065001, arXiv:1608.04784 [hep-ph].
- [24] ALICE Collaboration, S. Acharya *et al.*, “Constraints on jet quenching in p–Pb collisions at $\sqrt{s_{NN}} = 5.02$ TeV measured by the event-activity dependence of semi-inclusive hadron-jet distributions”, *Phys. Lett. B* **783** (2018) 95–113, arXiv:1712.05603 [nucl-ex].
- [25] ATLAS Collaboration, G. Aad *et al.*, “Strong Constraints on Jet Quenching in Centrality-Dependent p+Pb Collisions at 5.02 TeV from ATLAS”, *Phys. Rev. Lett.* **131** (2023) 072301, arXiv:2206.01138 [nucl-ex].
- [26] CMS Collaboration, V. Khachatryan *et al.*, “Observation of Long-Range Near-Side Angular Correlations in Proton-Proton Collisions at the LHC”, *JHEP* **09** (2010) 091, arXiv:1009.4122 [hep-ex].
- [27] ATLAS Collaboration, G. Aad *et al.*, “Observation of Long-Range Elliptic Azimuthal Anisotropies in $\sqrt{s} = 13$ and 2.76 TeV pp Collisions with the ATLAS Detector”, *Phys. Rev. Lett.* **116** (2016) 172301, arXiv:1509.04776 [hep-ex].
- [28] ATLAS Collaboration, M. Aaboud *et al.*, “Measurements of long-range azimuthal anisotropies and associated Fourier coefficients for pp collisions at $\sqrt{s} = 5.02$ and 13 TeV and p +Pb collisions at $\sqrt{s_{NN}} = 5.02$ TeV with the ATLAS detector”, *Phys. Rev. C* **96** (2017) 024908, arXiv:1609.06213 [nucl-ex].
- [29] CMS Collaboration, V. Khachatryan *et al.*, “Evidence for collectivity in pp collisions at the LHC”, *Phys. Lett. B* **765** (2017) 193–220, arXiv:1606.06198 [nucl-ex].
- [30] CMS Collaboration, S. Chatrchyan *et al.*, “Observation of Long-Range Near-Side Angular Correlations in Proton-Lead Collisions at the LHC”, *Phys. Lett. B* **718** (2013) 795–814, arXiv:1210.5482 [nucl-ex].
- [31] ALICE Collaboration, J. Adam *et al.*, “Enhanced production of multi-strange hadrons in high-multiplicity proton-proton collisions”, *Nature Phys.* **13** (2017) 535–539, arXiv:1606.07424 [nucl-ex].
- [32] ALICE Collaboration, S. Acharya *et al.*, “Multiplicity dependence of (multi-)strange hadron production in proton-proton collisions at $\sqrt{s} = 13$ TeV”, *Eur. Phys. J. C* **80** (2020) 167, arXiv:1908.01861 [nucl-ex].
- [33] ALICE Collaboration, J. Adam *et al.*, “Multi-strange baryon production in p–Pb collisions at $\sqrt{s_{NN}} = 5.02$ TeV”, *Phys. Lett. B* **758** (2016) 389–401, arXiv:1512.07227 [nucl-ex].
- [34] CMS Collaboration, V. Khachatryan *et al.*, “Evidence for collectivity in pp collisions at the LHC”, *Phys. Lett. B* **765** (2017) 193–220, arXiv:1606.06198 [nucl-ex].
- [35] ATLAS Collaboration, G. Aad *et al.*, “Measurement of azimuthal anisotropy of muons from charm and bottom hadrons in pp collisions at $\sqrt{s} = 13$ TeV with the ATLAS detector”, *Phys. Rev. Lett.* **124** (2020) 082301, arXiv:1909.01650 [nucl-ex].

- [36] **ALICE** Collaboration, J. Adam *et al.*, “Measurement of charged jet production cross sections and nuclear modification in p–Pb collisions at $\sqrt{s_{NN}} = 5.02$ TeV”, *Phys. Lett. B* **749** (2015) 68–81, arXiv:1503.00681 [nucl-ex].
- [37] **ALICE** Collaboration, J. Adam *et al.*, “Centrality dependence of charged jet production in p–Pb collisions at $\sqrt{s_{NN}} = 5.02$ TeV”, *Eur. Phys. J. C* **76** (2016) 271, arXiv:1603.03402 [nucl-ex].
- [38] M. H. Seymour, “Jet shapes in hadron collisions: Higher orders, resummation and hadronization”, *Nucl. Phys. B* **513** (1998) 269–300, arXiv:hep-ph/9707338.
- [39] I. Vitev, S. Wicks, and B.-W. Zhang, “A Theory of jet shapes and cross sections: From hadrons to nuclei”, *JHEP* **11** (2008) 093, arXiv:0810.2807 [hep-ph].
- [40] A. H. Mueller, “On the Multiplicity of Hadrons in QCD Jets”, *Phys. Lett. B* **104** (1981) 161–164.
- [41] S. D. Ellis, Z. Kunszt, and D. E. Soper, “Jets at hadron colliders at order $\alpha - s^3$: A Look inside”, *Phys. Rev. Lett.* **69** (1992) 3615–3618, arXiv:hep-ph/9208249.
- [42] **CDF** Collaboration, T. Affolder *et al.*, “Charged Jet Evolution and the Underlying Event in $p\bar{p}$ Collisions at 1.8 TeV”, *Phys. Rev. D* **65** (2002) 092002.
- [43] **CDF** Collaboration, D. Acosta *et al.*, “Study of jet shapes in inclusive jet production in $p\bar{p}$ collisions at $\sqrt{s} = 1.96$ TeV”, *Phys. Rev. D* **71** (2005) 112002, arXiv:hep-ex/0505013.
- [44] **D0** Collaboration, S. Abachi *et al.*, “Transverse energy distributions within jets in $p\bar{p}$ collisions at $\sqrt{s} = 1.8$ TeV”, *Phys. Lett. B* **357** (1995) 500–508.
- [45] **ATLAS** Collaboration, G. Aad *et al.*, “Study of Jet Shapes in Inclusive Jet Production in pp Collisions at $\sqrt{s} = 7$ TeV using the ATLAS Detector”, *Phys. Rev. D* **83** (2011) 052003, arXiv:1101.0070 [hep-ex].
- [46] **ATLAS** Collaboration, G. Aad *et al.*, “Properties of jet fragmentation using charged particles measured with the ATLAS detector in pp collisions at $\sqrt{s} = 13$ TeV”, *Phys. Rev. D* **100** (2019) 052011, arXiv:1906.09254 [hep-ex].
- [47] **CMS** Collaboration, S. Chatrchyan *et al.*, “Shape, Transverse Size, and Charged Hadron Multiplicity of Jets in pp Collisions at 7 TeV”, *JHEP* **06** (2012) 160, arXiv:1204.3170 [hep-ex].
- [48] **CMS** Collaboration, S. Chatrchyan *et al.*, “Modification of Jet Shapes in PbPb Collisions at $\sqrt{s_{NN}} = 2.76$ TeV”, *Phys. Lett. B* **730** (2014) 243–263, arXiv:1310.0878 [nucl-ex].
- [49] **CDF** Collaboration, D. Acosta *et al.*, “Momentum Distribution of Charged Particles in Jets in Dijet Events in $p\bar{p}$ Collisions at $\sqrt{s} = 1.8$ TeV and Comparisons to Perturbative QCD Predictions”, *Phys. Rev. D* **68** (2003) 012003.
- [50] **ATLAS** Collaboration, G. Aad *et al.*, “Measurement of the jet fragmentation function and transverse profile in proton-proton collisions at a center-of-mass energy of 7 TeV with the ATLAS detector”, *Eur. Phys. J. C* **71** (2011) 1795, arXiv:1109.5816 [hep-ex].
- [51] **ATLAS** Collaboration, G. Aad *et al.*, “Measurement of inclusive jet charged-particle fragmentation functions in Pb+Pb collisions at $\sqrt{s_{NN}} = 2.76$ TeV with the ATLAS detector”, *Phys. Lett. B* **739** (2014) 320–342, arXiv:1406.2979 [hep-ex].
- [52] **CMS** Collaboration, S. Chatrchyan *et al.*, “Measurement of jet fragmentation into charged particles in pp and PbPb collisions at $\sqrt{s_{NN}} = 2.76$ TeV”, *JHEP* **10** (2012) 087, arXiv:1205.5872 [nucl-ex].

- [53] D. Neill, F. Ringer, and N. Sato, “Leading jets and energy loss”, *JHEP* **07** (2021) 041, arXiv:2103.16573 [hep-ph].
- [54] ALICE Collaboration, K. Aamodt *et al.*, “The ALICE experiment at the CERN LHC”, *JINST* **3** (2008) S08002.
- [55] ALICE Collaboration, B. B. Abelev *et al.*, “Performance of the ALICE Experiment at the CERN LHC”, *Int. J. Mod. Phys. A* **29** (2014) 1430044, arXiv:1402.4476 [nucl-ex].
- [56] ALICE Collaboration, E. Abbas *et al.*, “Performance of the ALICE VZERO system”, *JINST* **8** (2013) P10016, arXiv:1306.3130 [nucl-ex].
- [57] ALICE Collaboration, S. Acharya *et al.*, “Search for jet quenching effects in high-multiplicity pp collisions at $\sqrt{s} = 13$ TeV via di-jet acoplanarity”, arXiv:2309.03788 [hep-ex].
- [58] ALICE Collaboration, S. Acharya *et al.*, “Pseudorapidity distributions of charged particles as a function of mid- and forward rapidity multiplicities in pp collisions at $\sqrt{s} = 5.02, 7$ and 13 TeV”, *Eur. Phys. J. C* **81** (2021) 630, arXiv:2009.09434 [nucl-ex].
- [59] ALICE Collaboration, S. Acharya *et al.*, “Multiplicity dependence of charged-particle jet production in pp collisions at $\sqrt{s} = 13$ TeV”, *Eur. Phys. J. C* **82** (2022) 514, arXiv:2202.01548 [nucl-ex].
- [60] ALICE Collaboration, “The ALICE definition of primary particles”, *ALICE-PUBLIC-2017-005* (2017). <https://cds.cern.ch/record/2270008>.
- [61] ALICE Collaboration, S. Acharya *et al.*, “Measurements of inclusive jet spectra in pp and central Pb–Pb collisions at $\sqrt{s_{NN}} = 5.02$ TeV”, *Phys. Rev. C* **101** (2020) 034911, arXiv:1909.09718 [nucl-ex].
- [62] T. Sjöstrand *et al.*, “An introduction to PYTHIA 8.2”, *Comput. Phys. Commun.* **191** (2015) 159–177, arXiv:1410.3012 [hep-ph].
- [63] P. Skands, S. Carrazza, and J. Rojo, “Tuning PYTHIA 8.1: the Monash 2013 Tune”, *Eur. Phys. J. C* **74** (2014) 3024, arXiv:1404.5630 [hep-ph].
- [64] T. Pierog, I. Karpenko, J. M. Katzy, E. Yatsenko, and K. Werner, “EPOS LHC: Test of collective hadronization with data measured at the CERN Large Hadron Collider”, *Phys. Rev. C* **92** (2015) 034906, arXiv:1306.0121 [hep-ph].
- [65] M. Cacciari, G. P. Salam, and G. Soyez, “The anti- k_t jet clustering algorithm”, *JHEP* **04** (2008) 063, arXiv:0802.1189 [hep-ph].
- [66] M. Cacciari, G. P. Salam, and G. Soyez, “FastJet User Manual”, *Eur. Phys. J. C* **72** (2012) 1896, arXiv:1111.6097 [hep-ph].
- [67] R. Brun *et al.*, “*GEANT: Detector Description and Simulation Tool*”. CERN Program Library. CERN, Geneva, 1993. <http://cds.cern.ch/record/1082634>.
- [68] B. I. Ermolaev and V. S. Fadin, “Log - Log Asymptotic Form of Exclusive Cross-Sections in Quantum Chromodynamics”, *JETP Lett.* **33** (1981) 269–272.
- [69] G. D’Agostini, “Improved iterative Bayesian unfolding”, in *Alliance Workshop on Unfolding and Data Correction*. 10, 2010. arXiv:1010.0632 [physics.data-an].
- [70] T. Auye, “Unfolding algorithms and tests using RooUnfold”, in *PHYSTAT 2011*, pp. 313–318. CERN, Geneva, 2011. arXiv:1105.1160 [physics.data-an].















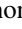




- [71] **ALICE** Collaboration, S. Acharya *et al.*, “Underlying Event properties in pp collisions at $\sqrt{s} = 13$ TeV”, *JHEP* **04** (2020) 192, arXiv:1910.14400 [nucl-ex].
- [72] **ALICE** Collaboration, S. Acharya *et al.*, “First measurements of N-subjettiness in central Pb–Pb collisions at $\sqrt{s_{NN}} = 2.76$ TeV”, *JHEP* **10** (2021) 003, arXiv:2105.04936 [nucl-ex].
- [73] **CMS** Collaboration, S. Chatrchyan *et al.*, “Jet and Underlying Event Properties as a Function of Charged-Particle Multiplicity in Proton–Proton Collisions at $\sqrt{s} = 7$ TeV”, *Eur. Phys. J. C* **73** (2013) 2674, arXiv:1310.4554 [hep-ex].
- [74] Z. Varga, R. Vártesi, and G. Gábor Barnaföldi, “Modification of jet structure in high-multiplicity pp collisions due to multiple-parton interactions and observing a multiplicity-independent characteristic jet size”, *Adv. High Energy Phys.* **2019** (2019) 6731362, arXiv:1805.03101 [hep-ph].
- [75] C. Bierlich, S. Chakraborty, G. Gustafson, and L. Lönnblad, “Jet modifications from colour rope formation in dense systems of non-parallel strings”, *SciPost Phys.* **13** (2022) 023, arXiv:2202.12783 [hep-ph].
- [76] P. Das, A. Modak, D. Banerjee, R. Biswas, S. Das, S. K. Ghosh, S. Raha, and S. K. Prasad, “Jet modification in absence of QGP-medium: the role of multiparton interactions and color reconnection”, arXiv:2209.00972 [hep-ph].

A The ALICE Collaboration

S. Acharya ¹²⁷, D. Adamová ⁸⁶, G. Aglieri Rinella ³³, M. Agnello ³⁰, N. Agrawal ⁵², Z. Ahammed ¹³⁵, S. Ahmad ¹⁶, S.U. Ahn ⁷², I. Ahuja ³⁸, A. Akhmedov ¹⁴¹, M. Al-Turany ⁹⁷, D. Aleksandrov ¹⁴¹, B. Alessandro ⁵⁷, H.M. Alfanda ⁶, R. Alfaro Molina ⁶⁸, B. Ali ¹⁶, A. Alici ²⁶, N. Alizadehvandchali ¹¹⁶, A. Alkin ³³, J. Alme ²¹, G. Alocco ⁵³, T. Alt ⁶⁵, A.R. Altamura ⁵¹, I. Altsybeev ⁹⁵, J.R. Alvarado ⁴⁵, M.N. Anaam ⁶, C. Andrei ⁴⁶, N. Andreou ¹¹⁵, A. Andronic ¹²⁶, E. Andronov ¹⁴¹, V. Anguelov ⁹⁴, F. Antinori ⁵⁵, P. Antonioli ⁵², N. Apadula ⁷⁴, L. Aphecetche ¹⁰³, H. Appelshäuser ⁶⁵, C. Arata ⁷³, S. Arcelli ²⁶, M. Aresti ²³, R. Arnaldi ⁵⁷, J.G.M.C.A. Arneiro ¹¹⁰, I.C. Arsene ²⁰, M. Arslandok ¹³⁸, A. Augustinus ³³, R. Averbeck ⁹⁷, M.D. Azmi ¹⁶, H. Baba ¹²⁴, A. Badalà ⁵⁴, J. Bae ¹⁰⁴, Y.W. Baek ⁴¹, X. Bai ¹²⁰, R. Bailhache ⁶⁵, Y. Bailung ⁴⁹, R. Bala ⁹¹, A. Balbino ³⁰, A. Baldisseri ¹³⁰, B. Balis ², D. Banerjee ⁴, Z. Banoo ⁹¹, F. Barile ³², L. Barioglio ⁵⁷, M. Barlou ⁷⁸, B. Barman ⁴², G.G. Barnaföldi ⁴⁷, L.S. Barnby ⁸⁵, E. Barreau ¹⁰³, V. Barret ¹²⁷, L. Barreto ¹¹⁰, C. Bartels ¹¹⁹, K. Barth ³³, E. Bartsch ⁶⁵, N. Bastid ¹²⁷, S. Basu ⁷⁵, G. Batigne ¹⁰³, D. Battistini ⁹⁵, B. Batyunya ¹⁴², D. Bauri ⁴⁸, J.L. Bazo Alba ¹⁰¹, I.G. Bearden ⁸³, C. Beattie ¹³⁸, P. Becht ⁹⁷, D. Behera ⁴⁹, I. Belikov ¹²⁹, A.D.C. Bell Hechavarria ¹²⁶, F. Bellini ²⁶, R. Bellwied ¹¹⁶, S. Belokurova ¹⁴¹, L.G.E. Beltran ¹⁰⁹, Y.A.V. Beltran ⁴⁵, G. Bencedi ⁴⁷, S. Beole ²⁵, Y. Berdnikov ¹⁴¹, A. Berdnikova ⁹⁴, L. Bergmann ⁹⁴, M.G. Besoiu ⁶⁴, L. Betev ³³, P.P. Bhaduri ¹³⁵, A. Bhasin ⁹¹, M.A. Bhat ⁴, B. Bhattacharjee ⁴², L. Bianchi ²⁵, N. Bianchi ⁵⁰, J. Bielčik ³⁶, J. Bielčíková ⁸⁶, A.P. Bigot ¹²⁹, A. Bilandzic ⁹⁵, G. Biro ⁴⁷, S. Biswas ⁴, N. Bize ¹⁰³, J.T. Blair ¹⁰⁸, D. Blau ¹⁴¹, M.B. Blidaru ⁹⁷, N. Bluhme ³⁹, C. Blume ⁶⁵, G. Boca ^{22,56}, F. Bock ⁸⁷, T. Bodova ²¹, S. Boi ²³, J. Bok ¹⁷, L. Boldizsár ⁴⁷, M. Bombara ³⁸, P.M. Bond ³³, G. Bonomi ^{134,56}, H. Borel ¹³⁰, A. Borissov ¹⁴¹, A.G. Borquez Carcamo ⁹⁴, H. Bossi ¹³⁸, E. Botta ²⁵, Y.E.M. Bouziani ⁶⁵, L. Bratrud ⁶⁵, P. Braun-Munzinger ⁹⁷, M. Bregant ¹¹⁰, M. Broz ³⁶, G.E. Bruno ^{96,32}, M.D. Buckland ²⁴, D. Budnikov ¹⁴¹, H. Buesching ⁶⁵, S. Bufalino ³⁰, P. Buhler ¹⁰², N. Burmasov ¹⁴¹, Z. Buthelezi ^{69,123}, A. Bylinkin ²¹, S.A. Bysiak ¹⁰⁷, J.C. Cabanillas Noris ¹⁰⁹, M. Cai ⁶, H. Caines ¹³⁸, A. Caliva ²⁹, E. Calvo Villar ¹⁰¹, J.M.M. Camacho ¹⁰⁹, P. Camerini ²⁴, F.D.M. Canedo ¹¹⁰, S.L. Cantway ¹³⁸, M. Carabas ¹¹³, A.A. Carballo ³³, F. Carnesecchi ³³, R. Caron ¹²⁸, L.A.D. Carvalho ¹¹⁰, J. Castillo Castellanos ¹³⁰, F. Catalano ^{33,25}, S. Cattaruzzi ²⁴, C. Ceballos Sanchez ¹⁴², I. Chakaberia ⁷⁴, P. Chakraborty ⁴⁸, S. Chandra ¹³⁵, S. Chapeland ³³, M. Chartier ¹¹⁹, S. Chattopadhyay ¹³⁵, S. Chattopadhyay ⁹⁹, T. Cheng ^{97,6}, C. Cheshkov ¹²⁸, V. Chibante Barroso ³³, D.D. Chinellato ¹¹¹, E.S. Chizzali ^{11,95}, J. Cho ⁵⁹, S. Cho ⁵⁹, P. Chochula ³³, D. Choudhury ⁴², P. Christakoglou ⁸⁴, C.H. Christensen ⁸³, P. Christiansen ⁷⁵, T. Chujo ¹²⁵, M. Ciaccio ³⁰, C. Cicalo ⁵³, M.R. Ciupek ⁹⁷, G. Clai ^{III,52}, F. Colamaria ⁵¹, J.S. Colburn ¹⁰⁰, D. Colella ^{96,32}, M. Colocci ²⁶, M. Concas ^{IV,33}, G. Conesa Balbastre ⁷³, Z. Conesa del Valle ¹³¹, G. Contin ²⁴, J.G. Contreras ³⁶, M.L. Coquet ¹³⁰, P. Cortese ^{133,57}, M.R. Cosentino ¹¹², F. Costa ³³, S. Costanza ^{22,56}, C. Cot ¹³¹, J. Crkovská ⁹⁴, P. Crochet ¹²⁷, R. Cruz-Torres ⁷⁴, P. Cui ⁶, A. Dainese ⁵⁵, M.C. Danisch ⁹⁴, A. Danu ⁶⁴, P. Das ⁸⁰, P. Das ⁴, S. Das ⁴, A.R. Dash ¹²⁶, S. Dash ⁴⁸, A. De Caro ²⁹, G. de Cataldo ⁵¹, J. de Cuveland ³⁹, A. De Falco ²³, D. De Gruttola ²⁹, N. De Marco ⁵⁷, C. De Martin ²⁴, S. De Pasquale ²⁹, R. Deb ¹³⁴, R. Del Grande ⁹⁵, L. Dello Stritto ^{33,29}, W. Deng ⁶, P. Dhankher ¹⁹, D. Di Bari ³², A. Di Mauro ³³, B. Diab ¹³⁰, R.A. Diaz ^{142,7}, T. Dietel ¹¹⁴, Y. Ding ⁶, J. Ditzel ⁶⁵, R. Divià ³³, D.U. Dixit ¹⁹, Ø. Djuvsland ²¹, U. Dmitrieva ¹⁴¹, A. Dobrin ⁶⁴, B. Dönigus ⁶⁵, J.M. Dubinski ¹³⁶, A. Dubla ⁹⁷, S. Dudi ⁹⁰, P. Dupieux ¹²⁷, M. Durkac ¹⁰⁶, N. Dzalaiova ¹³, T.M. Eder ¹²⁶, R.J. Ehlers ⁷⁴, F. Eisenhut ⁶⁵, R. Ejima ⁹², D. Elia ⁵¹, B. Erazmus ¹⁰³, F. Ercolessi ²⁶, B. Espagnon ¹³¹, G. Eulisse ³³, D. Evans ¹⁰⁰, S. Evdokimov ¹⁴¹, L. Fabbietti ⁹⁵, M. Faggin ²⁸, J. Faivre ⁷³, F. Fan ⁶, W. Fan ⁷⁴, A. Fantoni ⁵⁰, M. Fasel ⁸⁷, A. Feliciello ⁵⁷, G. Feofilov ¹⁴¹, A. Fernández Téllez ⁴⁵, L. Ferrandi ¹¹⁰, M.B. Ferrer ³³, A. Ferrero ¹³⁰, C. Ferrero ⁵⁷, A. Ferretti ²⁵, V.J.G. Feuillard ⁹⁴, V. Filova ³⁶, D. Finogeev ¹⁴¹, F.M. Fionda ⁵³, E. Flatland ³³, F. Flor ¹¹⁶, A.N. Flores ¹⁰⁸, S. Foertsch ⁶⁹, I. Fokin ⁹⁴, S. Fokin ¹⁴¹, E. Fragiaco ⁵⁸, E. Frajna ⁴⁷, U. Fuchs ³³, N. Funicello ²⁹, C. Furget ⁷³, A. Furs ¹⁴¹, T. Fusayasu ⁹⁸, J.J. Gaardhøje ⁸³, M. Gagliardi ²⁵, A.M. Gago ¹⁰¹, T. Gahlaut ¹⁰⁹, C.D. Galvan ¹⁰⁹, D.R. Gangadharan ¹¹⁶, P. Ganoti ⁷⁸, C. Garabatos ⁹⁷, T. García Chávez ⁴⁵, E. Garcia-Solis ⁹, C. Gargiulo ³³, P. Gasik ⁹⁷, A. Gautam ¹¹⁸, M.B. Gay Ducati ⁶⁷, M. Germain ¹⁰³, A. Ghimouz ¹²⁵, C. Ghosh ¹³⁵, M. Giacalone ⁵², G. Gioachin ³⁰, P. Giubellino ^{97,57}, P. Giubilato ²⁸, A.M.C. Glaenzer ¹³⁰, P. Glässel ⁹⁴, E. Glimos ¹²², D.J.Q. Goh ⁷⁶, V. Gonzalez ¹³⁷, P. Gordeev ¹⁴¹, M. Gorgon ², K. Goswami ⁴⁹, S. Gotovac ³⁴, V. Grabski ⁶⁸, L.K. Graczykowski ¹³⁶, E. Grecka ⁸⁶, A. Grelli ⁶⁰, C. Grigoras ³³, V. Grigoriev ¹⁴¹, S. Grigoryan ^{142,1}, F. Grosa ³³, J.F. Grosse-Oetringhaus ³³, R. Grosso ⁹⁷, D. Grund ³⁶, N.A. Grunwald ⁹⁴, G.G. Guardiani ¹¹¹, R. Guernane ⁷³, M. Guilbaud ¹⁰³, K. Gulbrandsen ⁸³, T. Gündem ⁶⁵, T. Gunji ¹²⁴,

W. Guo⁶, A. Gupta⁹¹, R. Gupta⁹¹, R. Gupta⁴⁹, K. Gwizdziel¹³⁶, L. Gyulai⁴⁷, C. Hadjidakis¹³¹, F.U. Haider⁹¹, S. Haidlova³⁶, M. Haldar⁴, H. Hamagaki⁷⁶, A. Hamdi⁷⁴, Y. Han¹³⁹, B.G. Hanley¹³⁷, R. Hannigan¹⁰⁸, J. Hansen⁷⁵, J.W. Harris¹³⁸, A. Harton⁹, M.V. Hartung⁶⁵, H. Hassan¹¹⁷, D. Hatzifotiadou⁵², P. Hauer⁴³, L.B. Havener¹³⁸, E. Hellbär⁹⁷, H. Helstrup³⁵, M. Hemmer⁶⁵, T. Herman³⁶, G. Herrera Corral⁸, F. Herrmann¹²⁶, S. Herrmann¹²⁸, K.F. Hetland³⁵, B. Heybeck⁶⁵, H. Hillemanns³³, B. Hippolyte¹²⁹, F.W. Hoffmann⁷¹, B. Hofman⁶⁰, G.H. Hong¹³⁹, M. Horst⁹⁵, A. Horzyk², Y. Hou⁶, P. Hristov³³, P. Huhn⁶⁵, L.M. Huhta¹¹⁷, T.J. Humanic⁸⁸, A. Hutson¹¹⁶, D. Hutter³⁹, M.C. Hwang¹⁹, R. Ilkaev¹⁴¹, H. Ilyas¹⁴, M. Inaba¹²⁵, G.M. Innocenti³³, M. Ippolitov¹⁴¹, A. Isakov⁸⁴, T. Isidori¹¹⁸, M.S. Islam⁹⁹, M. Ivanov⁹⁷, M. Ivanov¹³, V. Ivanov¹⁴¹, K.E. Iversen⁷⁵, M. Jablonski², B. Jacak^{19,74}, N. Jacazio²⁶, P.M. Jacobs⁷⁴, S. Jadlovská¹⁰⁶, J. Jadlovsky¹⁰⁶, S. Jaelani⁸², C. Jahnke¹¹⁰, M.J. Jakubowska¹³⁶, M.A. Janik¹³⁶, T. Janson⁷¹, S. Ji¹⁷, S. Jia¹⁰, A.A.P. Jimenez⁶⁶, F. Jonas^{74,87,126}, D.M. Jones¹¹⁹, J.M. Jowett^{33,97}, J. Jung⁶⁵, M. Jung⁶⁵, A. Junique³³, A. Jusko¹⁰⁰, M.J. Kabus^{33,136}, J. Kaewjai¹⁰⁵, P. Kalinak⁶¹, A.S. Kalteyer⁹⁷, A. Kalweit³³, D. Karatovic⁸⁹, O. Karavichev¹⁴¹, T. Karavicheva¹⁴¹, P. Karczmarczyk¹³⁶, E. Karpechev¹⁴¹, U. Kebschull⁷¹, R. Keidel¹⁴⁰, D.L.D. Keijdener⁶⁰, M. Keil³³, B. Ketzer⁴³, S.S. Khade⁴⁹, A.M. Khan¹²⁰, S. Khan¹⁶, A. Khanzadeev¹⁴¹, Y. Kharlov¹⁴¹, A. Khatun¹¹⁸, A. Khuntia³⁶, Z. Khuranova⁶⁵, B. Kileng³⁵, B. Kim¹⁰⁴, C. Kim¹⁷, D.J. Kim¹¹⁷, E.J. Kim⁷⁰, J. Kim¹³⁹, J. Kim⁵⁹, J. Kim⁷⁰, M. Kim¹⁹, S. Kim¹⁸, T. Kim¹³⁹, K. Kimura⁹², S. Kirsch⁶⁵, I. Kisel³⁹, S. Kiselev¹⁴¹, A. Kisiel¹³⁶, J.P. Kitowski², J.L. Klay⁵, J. Klein³³, S. Klein⁷⁴, C. Klein-Bösing¹²⁶, M. Kleiner⁶⁵, T. Klemenz⁹⁵, A. Kluge³³, C. Kobdaj¹⁰⁵, T. Kollegger⁹⁷, A. Kondratyev¹⁴², N. Kondratyeva¹⁴¹, J. Konig⁶⁵, S.A. Konigstorfer⁹⁵, P.J. Konopka³³, G. Kornakov¹³⁶, M. Korwieser⁹⁵, S.D. Koryciak², A. Kotliarov⁸⁶, N. Kovacic⁸⁹, V. Kovalenko¹⁴¹, M. Kowalski¹⁰⁷, V. Kozuharov³⁷, I. Králik⁶¹, A. Kravčáková³⁸, L. Krcal^{33,39}, M. Krivda^{100,61}, F. Krizek⁸⁶, K. Krizkova Gajdosova³³, M. Kroesen⁹⁴, M. Krüger⁶⁵, D.M. Krupova³⁶, E. Kryshen¹⁴¹, V. Kučera⁵⁹, C. Kuhn¹²⁹, P.G. Kuijer⁸⁴, T. Kumaoka¹²⁵, D. Kumar¹³⁵, L. Kumar⁹⁰, N. Kumar⁹⁰, S. Kumar³², S. Kundu³³, P. Kurashvili⁷⁹, A. Kurepin¹⁴¹, A.B. Kurepin¹⁴¹, A. Kuryakin¹⁴¹, S. Kushpil⁸⁶, V. Kuskov¹⁴¹, M. Kutyla¹³⁶, M.J. Kweon⁵⁹, Y. Kwon¹³⁹, S.L. La Pointe³⁹, P. La Rocca²⁷, A. Lakrathok¹⁰⁵, M. Lamanna³³, A.R. Landou⁷³, R. Langoy¹²¹, P. Larionov³³, E. Laudi³³, L. Lautner^{33,95}, R. Lavicka¹⁰², R. Lea^{134,56}, H. Lee¹⁰⁴, I. Legrand⁴⁶, G. Legras¹²⁶, J. Lehrbach³⁹, T.M. Lelek², R.C. Lemmon⁸⁵, I. León Monzón¹⁰⁹, M.M. Lesch⁹⁵, E.D. Lesser¹⁹, P. Lévai⁴⁷, X. Li¹⁰, B.E. Liang-gilman¹⁹, J. Lien¹²¹, R. Lietava¹⁰⁰, I. Likmeta¹¹⁶, B. Lim²⁵, S.H. Lim¹⁷, V. Lindenstruth³⁹, A. Lindner⁴⁶, C. Lippmann⁹⁷, D.H. Liu⁶, J. Liu¹¹⁹, G.S.S. Liveraro¹¹¹, I.M. Lofnes²¹, C. Loizides⁸⁷, S. Lokos¹⁰⁷, J. Lomker⁶⁰, P. Loncar³⁴, X. Lopez¹²⁷, E. López Torres⁷, P. Lu^{97,120}, F.V. Lugo⁶⁸, J.R. Luhder¹²⁶, M. Lunardon²⁸, G. Luparello⁵⁸, Y.G. Ma⁴⁰, M. Mager³³, A. Maire¹²⁹, E.M. Majerz², M.V. Makariev³⁷, M. Malaev¹⁴¹, G. Malfattore²⁶, N.M. Malik⁹¹, Q.W. Malik²⁰, S.K. Malik⁹¹, L. Malinina^{I,VII,142}, D. Mallick¹³¹, N. Mallick⁴⁹, G. Mandaglio^{31,54}, S.K. Mandal⁷⁹, V. Manko¹⁴¹, F. Manso¹²⁷, V. Manzari⁵¹, Y. Mao⁶, R.W. Marcjan², G.V. Margagliotti²⁴, A. Margotti⁵², A. Marín⁹⁷, C. Markert¹⁰⁸, P. Martinengo³³, M.I. Martínez⁴⁵, G. Martínez García¹⁰³, M.P.P. Martins¹¹⁰, S. Masciocchi⁹⁷, M. Masera²⁵, A. Masoni⁵³, L. Massacrier¹³¹, O. Massen⁶⁰, A. Mastroserio^{132,51}, O. Matonoha⁷⁵, S. Mattiazzo²⁸, A. Matyja¹⁰⁷, C. Mayer¹⁰⁷, A.L. Mazuecos³³, F. Mazzaschi²⁵, M. Mazzilli³³, J.E. Mdhuli¹²³, Y. Melikyan⁴⁴, A. Menchaca-Rocha⁶⁸, J.E.M. Mendez⁶⁶, E. Meninno¹⁰², A.S. Menon¹¹⁶, M. Meres¹³, Y. Miake¹²⁵, L. Micheletti³³, D.L. Mihaylov⁹⁵, K. Mikhaylov^{142,141}, D. Miśkowiec⁹⁷, A. Modak⁴, B. Mohanty⁸⁰, M. Mohisin Khan^{V,16}, M.A. Molander⁴⁴, S. Monira¹³⁶, C. Mordasini¹¹⁷, D.A. Moreira De Godoy¹²⁶, I. Morozov¹⁴¹, A. Morsch³³, T. Mrnjavac³³, V. Muccifora⁵⁰, S. Muhuri¹³⁵, J.D. Mulligan⁷⁴, A. Mulliri²³, M.G. Munhoz¹¹⁰, R.H. Munzer⁶⁵, H. Murakami¹²⁴, S. Murray¹¹⁴, L. Musa³³, J. Musinsky⁶¹, J.W. Myrcha¹³⁶, B. Naik¹²³, A.I. Nambrath¹⁹, B.K. Nandi⁴⁸, R. Nania⁵², E. Nappi⁵¹, A.F. Nassirpour¹⁸, A. Nath⁹⁴, C. Nattrass¹²², M.N. Naydenov³⁷, A. Neagu²⁰, A. Negru¹¹³, E. Nekrasova¹⁴¹, L. Nellen⁶⁶, R. Nepeivoda⁷⁵, S. Nese²⁰, G. Neskovic³⁹, N. Nicassio⁵¹, B.S. Nielsen⁸³, E.G. Nielsen⁸³, S. Nikolaev¹⁴¹, S. Nikulin¹⁴¹, V. Nikulin¹⁴¹, F. Noferini⁵², S. Noh¹², P. Nomokonov¹⁴², J. Norman¹¹⁹, N. Novitzky⁸⁷, P. Nowakowski¹³⁶, A. Nyanin¹⁴¹, J. Nystrand²¹, S. Oh¹⁸, A. Ohlson⁷⁵, V.A. Okorokov¹⁴¹, J. Oleniacz¹³⁶, A. Onnerstad¹¹⁷, C. Oppedisano⁵⁷, A. Ortiz Velasquez⁶⁶, J. Otwinowski¹⁰⁷, M. Oya⁹², K. Oyama⁷⁶, Y. Pachmayer⁹⁴, S. Padhan⁴⁸, D. Pagano^{134,56}, G. Paic⁶⁶, S. Paisano-Guzmán⁴⁵, A. Palasciano⁵¹, S. Panebianco¹³⁰, H. Park¹²⁵, H. Park¹⁰⁴, J. Park⁵⁹, J.E. Parkkila³³, Y. Patley⁴⁸, B. Paul²³, M.M.D.M. Paulino¹¹⁰,

H. Pei⁶, T. Peitzmann⁶⁰, X. Peng¹¹, M. Pennisi²⁵, S. Perciballi²⁵, D. Peresunko¹⁴¹, G.M. Perez⁷, Y. Pestov¹⁴¹, V. Petrov¹⁴¹, M. Petrovici⁴⁶, R.P. Pezzi^{103,67}, S. Piano⁵⁸, M. Pikna¹³, P. Pillot¹⁰³, O. Pinazza^{52,33}, L. Pinsky¹¹⁶, C. Pinto⁹⁵, S. Pisano⁵⁰, M. Płoskoń⁷⁴, M. Planinic⁸⁹, F. Pliquett⁶⁵, M.G. Poghosyan⁸⁷, B. Polichtchouk¹⁴¹, S. Politano³⁰, N. Poljak⁸⁹, A. Pop⁴⁶, S. Porteboeuf-Houssais¹²⁷, V. Pozdniakov¹⁴², I.Y. Pozos⁴⁵, K.K. Pradhan⁴⁹, S.K. Prasad⁴, S. Prasad⁴⁹, R. Preghenella⁵², F. Prino⁵⁷, C.A. Pruneau¹³⁷, I. Pshenichnov¹⁴¹, M. Puccio³³, S. Pucillo²⁵, Z. Pugelova¹⁰⁶, S. Qiu⁸⁴, L. Quaglia²⁵, S. Ragoni¹⁵, A. Rai¹³⁸, A. Rakotozafindrabe¹³⁰, L. Ramello^{133,57}, F. Rami¹²⁹, T.A. Rancien⁷³, M. Rasa²⁷, S.S. Räsänen⁴⁴, R. Rath⁵², M.P. Rauch²¹, I. Ravasenga³³, K.F. Read^{87,122}, C. Reckziegel¹¹², A.R. Redelbach³⁹, K. Redlich^{VI,79}, C.A. Reetz⁹⁷, H.D. Regules-Medel⁴⁵, A. Rehman²¹, F. Reidt³³, H.A. Reme-Ness³⁵, Z. Rescakova³⁸, K. Reygers⁹⁴, A. Riabov¹⁴¹, V. Riabov¹⁴¹, R. Ricci²⁹, M. Richter²⁰, A.A. Riedel⁹⁵, W. Riegler³³, A.G. Riffero²⁵, C. Ristea⁶⁴, M.V. Rodriguez³³, M. Rodríguez Cahuantzi⁴⁵, S.A. Rodríguez Ramírez⁴⁵, K. Røed²⁰, R. Rogalev¹⁴¹, E. Rogochaya¹⁴², T.S. Rogoschinski⁶⁵, D. Rohr³³, D. Röhrich²¹, P.F. Rojas⁴⁵, S. Rojas Torres³⁶, P.S. Rokita¹³⁶, G. Romanenko²⁶, F. Ronchetti⁵⁰, A. Rosano^{31,54}, E.D. Rosas⁶⁶, K. Roslon¹³⁶, A. Rossi⁵⁵, A. Roy⁴⁹, S. Roy⁴⁸, N. Rubini²⁶, D. Ruggiano¹³⁶, R. Rui²⁴, P.G. Russek², R. Russo⁸⁴, A. Rustamov⁸¹, E. Ryabinkin¹⁴¹, Y. Ryabov¹⁴¹, A. Rybicki¹⁰⁷, H. Rytönen¹¹⁷, J. Ryu¹⁷, W. Rzesza¹³⁶, O.A.M. Saariimaki⁴⁴, S. Sadhu³², S. Sadosky¹⁴¹, J. Saetre²¹, K. Šafařík³⁶, P. Saha⁴², S.K. Saha⁴, S. Saha⁸⁰, B. Sahoo⁴⁹, R. Sahoo⁴⁹, S. Sahoo⁶², D. Sahu⁴⁹, P.K. Sahu⁶², J. Saini¹³⁵, K. Sajdakova³⁸, S. Sakai¹²⁵, M.P. Salvan⁹⁷, S. Sambyal⁹¹, D. Samitz¹⁰², I. Sanna^{33,95}, T.B. Saramela¹¹⁰, D. Sarkar⁸³, P. Sarma⁴², V. Sarritzu²³, V.M. Sarti⁹⁵, M.H.P. Sas³³, S. Sawan⁸⁰, E. Scapparone⁵², J. Schambach⁸⁷, H.S. Scheid⁶⁵, C. Schiaua⁴⁶, R. Schicker⁹⁴, F. Schlepfer⁹⁴, A. Schmah⁹⁷, C. Schmidt⁹⁷, H.R. Schmidt⁹³, M.O. Schmidt³³, M. Schmidt⁹³, N.V. Schmidt⁸⁷, A.R. Schmier¹²², R. Schotter¹²⁹, A. Schröter³⁹, J. Schukraft³³, K. Schweda⁹⁷, G. Scioli²⁶, E. Scomparin⁵⁷, J.E. Seger¹⁵, Y. Sekiguchi¹²⁴, D. Sekihata¹²⁴, M. Selina⁸⁴, I. Selyuzhenkov⁹⁷, S. Senyukov¹²⁹, J.J. Seo⁹⁴, D. Serebryakov¹⁴¹, L. Serkin⁶⁶, L. Šerkšnytė⁹⁵, A. Sevcenco⁶⁴, T.J. Shaba⁶⁹, A. Shabetai¹⁰³, R. Shahoyan³³, A. Shangaraev¹⁴¹, B. Sharma⁹¹, D. Sharma⁴⁸, H. Sharma⁵⁵, M. Sharma⁹¹, S. Sharma⁷⁶, S. Sharma⁹¹, U. Sharma⁹¹, A. Shatat¹³¹, O. Sheibani¹¹⁶, K. Shigaki⁹², M. Shimomura⁷⁷, J. Shin¹², S. Shirinkin¹⁴¹, Q. Shou⁴⁰, Y. Sibiriak¹⁴¹, S. Siddhanta⁵³, T. Siemiarczuk⁷⁹, T.F. Silva¹¹⁰, D. Silvermyr⁷⁵, T. Simantathammakul¹⁰⁵, R. Simeonov³⁷, B. Singh⁹¹, B. Singh⁹⁵, K. Singh⁴⁹, R. Singh⁸⁰, R. Singh⁹¹, R. Singh⁴⁹, S. Singh¹⁶, V.K. Singh¹³⁵, V. Singhal¹³⁵, T. Sinha⁹⁹, B. Sitar¹³, M. Sitta^{133,57}, T.B. Skaali²⁰, G. Skorodumovs⁹⁴, M. Slupecki⁴⁴, N. Smirnov¹³⁸, R.J.M. Snellings⁶⁰, E.H. Solheim²⁰, J. Song¹⁷, C. Sonnabend^{33,97}, J.M. Sonneveld⁸⁴, F. Soramel²⁸, A.B. Soto-herandez⁸⁸, R. Spijkers⁸⁴, I. Sputowska¹⁰⁷, J. Staa⁷⁵, J. Stachel⁹⁴, I. Stan⁶⁴, P.J. Steffanic¹²², S.F. Stiefelmaier⁹⁴, D. Stocco¹⁰³, I. Storehaug²⁰, P. Stratmann¹²⁶, S. Strazzi²⁶, A. Sturmiolo^{31,54}, C.P. Stylianidis⁸⁴, A.A.P. Suaide¹¹⁰, C. Suire¹³¹, M. Sukhanov¹⁴¹, M. Suljic³³, R. Sultanov¹⁴¹, V. Sumberia⁹¹, S. Sumowidagdo⁸², I. Szarka¹³, M. Szymkowski¹³⁶, S.F. Taghavi⁹⁵, G. Taillepied⁹⁷, J. Takahashi¹¹¹, G.J. Tambave⁸⁰, S. Tang⁶, Z. Tang¹²⁰, J.D. Tapia Takaki¹¹⁸, N. Tapus¹¹³, L.A. Tarasovicova¹²⁶, M.G. Tazila⁴⁶, G.F. Tassielli³², A. Tauro³³, A. Tavira García¹³¹, G. Tejeda Muñoz⁴⁵, A. Telesca³³, L. Terlizzi²⁵, C. Terrevoli¹¹⁶, S. Thakur⁴, D. Thomas¹⁰⁸, A. Tikhonov¹⁴¹, N. Tiltmann^{33,126}, A.R. Timmins¹¹⁶, M. Tkacik¹⁰⁶, T. Tkacik¹⁰⁶, A. Toia⁶⁵, R. Tokumoto⁹², K. Tomohiro⁹², N. Topilskaya¹⁴¹, M. Toppi⁵⁰, T. Tork¹³¹, P.V. Torres⁶⁶, V.V. Torres¹⁰³, A.G. Torres Ramos³², A. Trifiró^{31,54}, A.S. Triolo^{33,31,54}, S. Tripathy⁵², T. Tripathy⁴⁸, S. Trogolo³³, V. Trubnikov³, W.H. Trzaska¹¹⁷, T.P. Trzcinski¹³⁶, A. Tumkin¹⁴¹, R. Turrisi⁵⁵, T.S. Tveter²⁰, K. Ullaland²¹, B. Ulukutlu⁹⁵, A. Uras¹²⁸, M. Urioni¹³⁴, G.L. Usai²³, M. Vala³⁸, N. Valle²², L.V.R. van Doremalen⁶⁰, M. van Leeuwen⁸⁴, C.A. van Veen⁹⁴, R.J.G. van Weelden⁸⁴, P. Vande Vyvre³³, D. Varga⁴⁷, Z. Varga⁴⁷, M. Vasileiou⁷⁸, A. Vasiliev¹⁴¹, O. Vázquez Doce⁵⁰, O. Vazquez Rueda¹¹⁶, V. Vechernin¹⁴¹, E. Vercellin²⁵, S. Vergara Limón⁴⁵, R. Verma⁴⁸, L. Vermunt⁹⁷, R. Vértesi⁴⁷, M. Verweij⁶⁰, L. Vickovic³⁴, Z. Vilakazi¹²³, O. Villalobos Baillie¹⁰⁰, A. Villani²⁴, A. Vinogradov¹⁴¹, T. Virgili²⁹, M.M.O. Virta¹¹⁷, V. Vislavicius⁷⁵, A. Vodopyanov¹⁴², B. Volkel³³, M.A. Völkl⁹⁴, S.A. Voloshin¹³⁷, G. Volpe³², B. von Haller³³, I. Vorobyev³³, N. Vozniuk¹⁴¹, J. Vrláková³⁸, J. Wan⁴⁰, C. Wang⁴⁰, D. Wang⁴⁰, Y. Wang⁴⁰, Y. Wang⁶, A. Wegrzynek³³, F.T. Weiglhofer³⁹, S.C. Wenzel³³, J.P. Wessels¹²⁶, J. Wiechula⁶⁵, J. Wikne²⁰, G. Wilk⁷⁹, J. Wilkinson⁹⁷, G.A. Willems¹²⁶, B. Windelband⁹⁴, M. Winn¹³⁰, J.R. Wright¹⁰⁸, W. Wu⁴⁰, Y. Wu¹²⁰, R. Xu⁶, A. Yadav⁴³, A.K. Yadav¹³⁵, Y. Yamaguchi⁹², S. Yang²¹, S. Yano⁹², E.R. Yeats¹⁹, Z. Yin⁶, I.-K. Yoo¹⁷, J.H. Yoon⁵⁹, H. Yu¹², S. Yuan²¹, A. Yuncu⁹⁴, V. Zaccolo²⁴,

C. Zampolli ³³, F. Zanone ⁹⁴, N. Zardoshti ³³, A. Zarochentsev ¹⁴¹, P. Závada ⁶³, N. Zaviyalov¹⁴¹, M. Zhalov ¹⁴¹, B. Zhang ⁶, C. Zhang ¹³⁰, L. Zhang ⁴⁰, S. Zhang ⁴⁰, X. Zhang ⁶, Y. Zhang¹²⁰, Z. Zhang ⁶, M. Zhao ¹⁰, V. Zhrebchevskii ¹⁴¹, Y. Zhi¹⁰, C. Zhong⁴⁰, D. Zhou ⁶, Y. Zhou ⁸³, J. Zhu ^{55,6}, Y. Zhu⁶, S.C. Zugravel ⁵⁷, N. Zurlo ^{134,56}

Affiliation Notes

^I Deceased

^{II} Also at: Max-Planck-Institut für Physik, Munich, Germany

^{III} Also at: Italian National Agency for New Technologies, Energy and Sustainable Economic Development (ENEA), Bologna, Italy

^{IV} Also at: Dipartimento DET del Politecnico di Torino, Turin, Italy

^V Also at: Department of Applied Physics, Aligarh Muslim University, Aligarh, India

^{VI} Also at: Institute of Theoretical Physics, University of Wrocław, Poland

^{VII} Also at: An institution covered by a cooperation agreement with CERN

Collaboration Institutes

¹ A.I. Alikhanyan National Science Laboratory (Yerevan Physics Institute) Foundation, Yerevan, Armenia

² AGH University of Krakow, Cracow, Poland

³ Bogolyubov Institute for Theoretical Physics, National Academy of Sciences of Ukraine, Kiev, Ukraine

⁴ Bose Institute, Department of Physics and Centre for Astroparticle Physics and Space Science (CAPSS), Kolkata, India

⁵ California Polytechnic State University, San Luis Obispo, California, United States

⁶ Central China Normal University, Wuhan, China

⁷ Centro de Aplicaciones Tecnológicas y Desarrollo Nuclear (CEADEN), Havana, Cuba

⁸ Centro de Investigación y de Estudios Avanzados (CINVESTAV), Mexico City and Mérida, Mexico

⁹ Chicago State University, Chicago, Illinois, United States

¹⁰ China Institute of Atomic Energy, Beijing, China

¹¹ China University of Geosciences, Wuhan, China

¹² Chungbuk National University, Cheongju, Republic of Korea

¹³ Comenius University Bratislava, Faculty of Mathematics, Physics and Informatics, Bratislava, Slovak Republic

¹⁴ COMSATS University Islamabad, Islamabad, Pakistan

¹⁵ Creighton University, Omaha, Nebraska, United States

¹⁶ Department of Physics, Aligarh Muslim University, Aligarh, India

¹⁷ Department of Physics, Pusan National University, Pusan, Republic of Korea

¹⁸ Department of Physics, Sejong University, Seoul, Republic of Korea

¹⁹ Department of Physics, University of California, Berkeley, California, United States

²⁰ Department of Physics, University of Oslo, Oslo, Norway

²¹ Department of Physics and Technology, University of Bergen, Bergen, Norway

²² Dipartimento di Fisica, Università di Pavia, Pavia, Italy

²³ Dipartimento di Fisica dell'Università and Sezione INFN, Cagliari, Italy

²⁴ Dipartimento di Fisica dell'Università and Sezione INFN, Trieste, Italy

²⁵ Dipartimento di Fisica dell'Università and Sezione INFN, Turin, Italy

²⁶ Dipartimento di Fisica e Astronomia dell'Università and Sezione INFN, Bologna, Italy

²⁷ Dipartimento di Fisica e Astronomia dell'Università and Sezione INFN, Catania, Italy

²⁸ Dipartimento di Fisica e Astronomia dell'Università and Sezione INFN, Padova, Italy

²⁹ Dipartimento di Fisica 'E.R. Caianiello' dell'Università and Gruppo Collegato INFN, Salerno, Italy

³⁰ Dipartimento DISAT del Politecnico and Sezione INFN, Turin, Italy

³¹ Dipartimento di Scienze MIFT, Università di Messina, Messina, Italy

³² Dipartimento Interateneo di Fisica 'M. Merlin' and Sezione INFN, Bari, Italy

³³ European Organization for Nuclear Research (CERN), Geneva, Switzerland

³⁴ Faculty of Electrical Engineering, Mechanical Engineering and Naval Architecture, University of Split, Split, Croatia

³⁵ Faculty of Engineering and Science, Western Norway University of Applied Sciences, Bergen, Norway

- ³⁶ Faculty of Nuclear Sciences and Physical Engineering, Czech Technical University in Prague, Prague, Czech Republic
- ³⁷ Faculty of Physics, Sofia University, Sofia, Bulgaria
- ³⁸ Faculty of Science, P.J. Šafárik University, Košice, Slovak Republic
- ³⁹ Frankfurt Institute for Advanced Studies, Johann Wolfgang Goethe-Universität Frankfurt, Frankfurt, Germany
- ⁴⁰ Fudan University, Shanghai, China
- ⁴¹ Gangneung-Wonju National University, Gangneung, Republic of Korea
- ⁴² Gauhati University, Department of Physics, Guwahati, India
- ⁴³ Helmholtz-Institut für Strahlen- und Kernphysik, Rheinische Friedrich-Wilhelms-Universität Bonn, Bonn, Germany
- ⁴⁴ Helsinki Institute of Physics (HIP), Helsinki, Finland
- ⁴⁵ High Energy Physics Group, Universidad Autónoma de Puebla, Puebla, Mexico
- ⁴⁶ Horia Hulubei National Institute of Physics and Nuclear Engineering, Bucharest, Romania
- ⁴⁷ HUN-REN Wigner Research Centre for Physics, Budapest, Hungary
- ⁴⁸ Indian Institute of Technology Bombay (IIT), Mumbai, India
- ⁴⁹ Indian Institute of Technology Indore, Indore, India
- ⁵⁰ INFN, Laboratori Nazionali di Frascati, Frascati, Italy
- ⁵¹ INFN, Sezione di Bari, Bari, Italy
- ⁵² INFN, Sezione di Bologna, Bologna, Italy
- ⁵³ INFN, Sezione di Cagliari, Cagliari, Italy
- ⁵⁴ INFN, Sezione di Catania, Catania, Italy
- ⁵⁵ INFN, Sezione di Padova, Padova, Italy
- ⁵⁶ INFN, Sezione di Pavia, Pavia, Italy
- ⁵⁷ INFN, Sezione di Torino, Turin, Italy
- ⁵⁸ INFN, Sezione di Trieste, Trieste, Italy
- ⁵⁹ Inha University, Incheon, Republic of Korea
- ⁶⁰ Institute for Gravitational and Subatomic Physics (GRASP), Utrecht University/Nikhef, Utrecht, Netherlands
- ⁶¹ Institute of Experimental Physics, Slovak Academy of Sciences, Košice, Slovak Republic
- ⁶² Institute of Physics, Homi Bhabha National Institute, Bhubaneswar, India
- ⁶³ Institute of Physics of the Czech Academy of Sciences, Prague, Czech Republic
- ⁶⁴ Institute of Space Science (ISS), Bucharest, Romania
- ⁶⁵ Institut für Kernphysik, Johann Wolfgang Goethe-Universität Frankfurt, Frankfurt, Germany
- ⁶⁶ Instituto de Ciencias Nucleares, Universidad Nacional Autónoma de México, Mexico City, Mexico
- ⁶⁷ Instituto de Física, Universidade Federal do Rio Grande do Sul (UFRGS), Porto Alegre, Brazil
- ⁶⁸ Instituto de Física, Universidad Nacional Autónoma de México, Mexico City, Mexico
- ⁶⁹ iThemba LABS, National Research Foundation, Somerset West, South Africa
- ⁷⁰ Jeonbuk National University, Jeonju, Republic of Korea
- ⁷¹ Johann-Wolfgang-Goethe Universität Frankfurt Institut für Informatik, Fachbereich Informatik und Mathematik, Frankfurt, Germany
- ⁷² Korea Institute of Science and Technology Information, Daejeon, Republic of Korea
- ⁷³ Laboratoire de Physique Subatomique et de Cosmologie, Université Grenoble-Alpes, CNRS-IN2P3, Grenoble, France
- ⁷⁴ Lawrence Berkeley National Laboratory, Berkeley, California, United States
- ⁷⁵ Lund University Department of Physics, Division of Particle Physics, Lund, Sweden
- ⁷⁶ Nagasaki Institute of Applied Science, Nagasaki, Japan
- ⁷⁷ Nara Women's University (NWU), Nara, Japan
- ⁷⁸ National and Kapodistrian University of Athens, School of Science, Department of Physics, Athens, Greece
- ⁷⁹ National Centre for Nuclear Research, Warsaw, Poland
- ⁸⁰ National Institute of Science Education and Research, Homi Bhabha National Institute, Jatni, India
- ⁸¹ National Nuclear Research Center, Baku, Azerbaijan
- ⁸² National Research and Innovation Agency - BRIN, Jakarta, Indonesia
- ⁸³ Niels Bohr Institute, University of Copenhagen, Copenhagen, Denmark
- ⁸⁴ Nikhef, National institute for subatomic physics, Amsterdam, Netherlands
- ⁸⁵ Nuclear Physics Group, STFC Daresbury Laboratory, Daresbury, United Kingdom
- ⁸⁶ Nuclear Physics Institute of the Czech Academy of Sciences, Husinec-Řež, Czech Republic
- ⁸⁷ Oak Ridge National Laboratory, Oak Ridge, Tennessee, United States

- 88 Ohio State University, Columbus, Ohio, United States
- 89 Physics department, Faculty of science, University of Zagreb, Zagreb, Croatia
- 90 Physics Department, Panjab University, Chandigarh, India
- 91 Physics Department, University of Jammu, Jammu, India
- 92 Physics Program and International Institute for Sustainability with Knotted Chiral Meta Matter (SKCM2), Hiroshima University, Hiroshima, Japan
- 93 Physikalisches Institut, Eberhard-Karls-Universität Tübingen, Tübingen, Germany
- 94 Physikalisches Institut, Ruprecht-Karls-Universität Heidelberg, Heidelberg, Germany
- 95 Physik Department, Technische Universität München, Munich, Germany
- 96 Politecnico di Bari and Sezione INFN, Bari, Italy
- 97 Research Division and ExtreMe Matter Institute EMMI, GSI Helmholtzzentrum für Schwerionenforschung GmbH, Darmstadt, Germany
- 98 Saga University, Saga, Japan
- 99 Saha Institute of Nuclear Physics, Homi Bhabha National Institute, Kolkata, India
- 100 School of Physics and Astronomy, University of Birmingham, Birmingham, United Kingdom
- 101 Sección Física, Departamento de Ciencias, Pontificia Universidad Católica del Perú, Lima, Peru
- 102 Stefan Meyer Institut für Subatomare Physik (SMI), Vienna, Austria
- 103 SUBATECH, IMT Atlantique, Nantes Université, CNRS-IN2P3, Nantes, France
- 104 Sungkyunkwan University, Suwon City, Republic of Korea
- 105 Suranaree University of Technology, Nakhon Ratchasima, Thailand
- 106 Technical University of Košice, Košice, Slovak Republic
- 107 The Henryk Niewodniczanski Institute of Nuclear Physics, Polish Academy of Sciences, Cracow, Poland
- 108 The University of Texas at Austin, Austin, Texas, United States
- 109 Universidad Autónoma de Sinaloa, Culiacán, Mexico
- 110 Universidade de São Paulo (USP), São Paulo, Brazil
- 111 Universidade Estadual de Campinas (UNICAMP), Campinas, Brazil
- 112 Universidade Federal do ABC, Santo Andre, Brazil
- 113 Universitatea Nationala de Stiinta si Tehnologie Politehnica Bucuresti, Bucharest, Romania
- 114 University of Cape Town, Cape Town, South Africa
- 115 University of Derby, Derby, United Kingdom
- 116 University of Houston, Houston, Texas, United States
- 117 University of Jyväskylä, Jyväskylä, Finland
- 118 University of Kansas, Lawrence, Kansas, United States
- 119 University of Liverpool, Liverpool, United Kingdom
- 120 University of Science and Technology of China, Hefei, China
- 121 University of South-Eastern Norway, Kongsberg, Norway
- 122 University of Tennessee, Knoxville, Tennessee, United States
- 123 University of the Witwatersrand, Johannesburg, South Africa
- 124 University of Tokyo, Tokyo, Japan
- 125 University of Tsukuba, Tsukuba, Japan
- 126 Universität Münster, Institut für Kernphysik, Münster, Germany
- 127 Université Clermont Auvergne, CNRS/IN2P3, LPC, Clermont-Ferrand, France
- 128 Université de Lyon, CNRS/IN2P3, Institut de Physique des 2 Infinis de Lyon, Lyon, France
- 129 Université de Strasbourg, CNRS, IPHC UMR 7178, F-67000 Strasbourg, France, Strasbourg, France
- 130 Université Paris-Saclay, Centre d'Etudes de Saclay (CEA), IRFU, Département de Physique Nucléaire (DPhN), Saclay, France
- 131 Université Paris-Saclay, CNRS/IN2P3, IJCLab, Orsay, France
- 132 Università degli Studi di Foggia, Foggia, Italy
- 133 Università del Piemonte Orientale, Vercelli, Italy
- 134 Università di Brescia, Brescia, Italy
- 135 Variable Energy Cyclotron Centre, Homi Bhabha National Institute, Kolkata, India
- 136 Warsaw University of Technology, Warsaw, Poland
- 137 Wayne State University, Detroit, Michigan, United States
- 138 Yale University, New Haven, Connecticut, United States
- 139 Yonsei University, Seoul, Republic of Korea
- 140 Zentrum für Technologie und Transfer (ZTT), Worms, Germany

¹⁴¹ Affiliated with an institute covered by a cooperation agreement with CERN

¹⁴² Affiliated with an international laboratory covered by a cooperation agreement with CERN.